Neutron-induced Fission

F. Gönnenwein

University of Tübingen / Germany

Abstract

Since the discovery of n-induced fission of uranium isotopes in 1939 a huge amount of data has been accumulated on the probability of the process and on the properties of fission fragments. Fission induced by neutrons in the actinides is the best studied reaction of nuclear physics. In the introduction of the present survey of the process first some basic notions relevant in fission are recalled. The main part of the paper is focused on the properties of fission fragments. Mass distributions of fragments are considered together with their interpretation in terms of symmetric, asymmetric and superasymmetric modes. Kinetic and excitation energies of fragments are discussed as a function of both, the nuclei undergoing fission and the fragment masses. In the nuclear charge distributions it is the even-odd staggering in the yields which is of major interest. Finally neutron and gamma emission from fragments are discussed. Their importance for the operation of nuclear power stations is highlighted.

1. Introduction

The reaction leading to the discovery of fission in January of 1939 by O. Hahn and F. Strassmann was neutron-induced fission of Uranium. In the process a heavy nucleus decays into two fragments of comparable mass. It was discussed by L Meitner in terms of a liquid drop which becomes deformed and which beyond a critical deformation is breaking apart into two pieces, the fission fragments. The fragments emit secondary neutrons. These neutrons may induce a second generation of fission events as the start of a chain reaction. The figure visualizes the process:

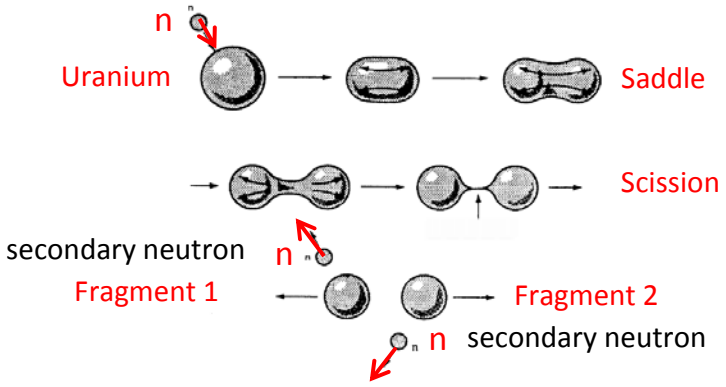

Fig.1: Scheme of neutron-induced fission

In the multidimensional landscape of deformation the critical deformation of no return to the mono-nucleus shows up as a saddle. With further deformation a situation is reached where the neck joining the two nascent fragments is no longer stable but is breaking apart. The snapping of the neck is called scission. Two fission fragments with similar but in general not equal masses are born. An obvious task in fission physics is hence the measurement of fragment mass and charge distributions. The fragments being charged the Coulomb forces will impart them large kinetic energies. The study of these energies is a further challenge.

As discovered by the team of F. Joliot and published in March 1939 secondary neutrons are created in fission. Finally, in the last stage of fission gammas are emitted.

In September 1939 N. Bohr and J.A. Wheeler published a seminal paper entitled “The Mechanism of Nuclear Fission”. Nuclear fission is interpreted in terms of the Liquid Drop Model. It is up to now the basis for understanding the process.

In the LDM the binding energy B of a nucleus (in MeV) is parameterized as

$$B = a_V A - a_S A^{2/3} - a_C Z^2/A^{1/3} - a_A (N-Z)^2/A \pm \delta/A^{1/2} \quad (1)$$

with the individual terms standing for the energies of Volume (A_V = 1.56), Surface (A_S = 17.23), Coulomb (a_C = 0.70), Asymmetry (a_A = 232.29) and Pairing (δ =’ 12.0MeV).

When the liquid drop becomes deformed, e.g. from a sphere to a spheroid, only the surface and the Coulomb energy are affected. Small deformations are described by developing the radius vector R(θ) of the nucleus

$$R(\theta) = R_0[1+\alpha_2 P_2(\cos\theta)] \quad (2)$$

with P_2 the second Legendre polynomial.

For small deformations α_2 Bohr-Wheeler calculate the surface and Coulomb energies E_S and E_C

$$E_S = E_S^0(1 + \tfrac{2}{5}\alpha_2^2) \text{ and } E_C = E_C^0(1 - \tfrac{1}{5}\alpha_2^2) \quad (3)$$

with E_S^0 and E_C^0 the energies for spherical nuclei as given by the LDM. For a spherical nucleus to be stable the decrease in Coulomb energy $\Delta E_C = -\tfrac{1}{5}\alpha_2^2 E_C^0$ must be smaller than the increase in surface energy $\Delta E_S = + \tfrac{2}{5}\alpha_2^2 E_S^0$ which for the limit of stability yields $|\Delta E_C| = \Delta E_S$ or $E_C^0 = 2E_S^0$. Bohr and Wheeler therefore introduce the notion of fissility x:

$$x = E_C^0 / 2\,E_S^0 = \text{—} / 51.7 \quad (4)$$

Only for x < 1 nuclei are stable against “immediate “decay within <10−19 s.

To calculate for large deformations the deformation energies requires to foresee in the expansion of R(θ) more Legendre polynomials than just P_2:

$$R(\theta) = R_0/\lambda \quad (5)$$

with λ a scale factor ensuring volume conservation.

Bohr-Wheeler succeeded to evaluate the potential energy of deformation as a function of the parameters α_2 and α_4. At small deformations the energy increases as expected. But the crucial discovery was that in the (α_2 , α_4) plane a saddle point is reached at specific α-parameter values. This is illustrated in Fig. 2. Beyond the saddle a path of minimum energy slopes downwards until the nucleus is breaking apart

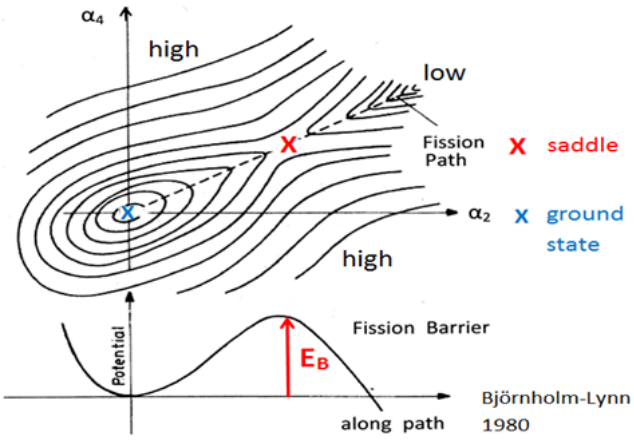

Fig. 2: Potential Energy Surface of a deforming nucleus

at scission. Fission proceeds along this path marked as a dashed line in the figure. A fissioning nucleus moving along the path has to overcome a potential barrier as shown in the lower part of the figure**. The** height of this "fission barrier" B_f above the ground state is about 6 MeV in the actinides. The fission barrier prevents heavy nuclei from immediate decay by fission.

However, similar to α-decay, the nucleus has a finite chance to tunnel through the barrier. "Spontaneous fission", as this process is called, was discovered for ^{238}U in 1940 by Flerov.

Fission induced by neutrons in actinide nuclei is the best studied fission reaction. Apart from its technological importance this is due to the exceptionally large cross sections for fission of nuclei like ^{235}U by thermal neutrons. The rate dN_f / dt of fission events in a flux of neutrons with density Φ_n is determined by the total number of irradiated target nuclei N_T and the fission cross section σ_f quoted in barns: 1 b = 10^{-28} m²:

$$dN_f / dt = \Phi_n N_T \sigma_f \qquad (6)$$

In the reaction ^{235}U(n_{th},f) with thermal neutrons of energy E_n = 25 meV the fission cross section σ_f = 586 b is huge: about 340 times the geometrical cross section of ^{236}U. The cross section is visualized in Fig. 3. Note its characteristic 1/ v dependence with a resonance structure superimposed.

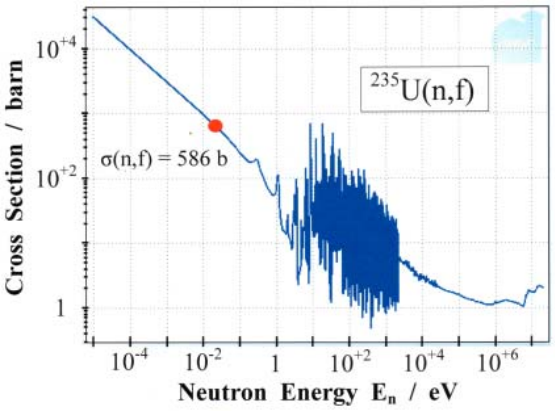

Fig. 3: Cross section for the ^{235}U(n,f) reaction

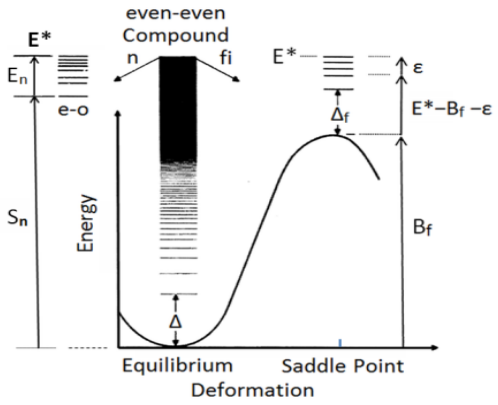

Fig. 4: Levels in the ground state and at the saddle point of a fissile nucleus

One of the reasons for the huge σ_f is the large neutron separation energy S_n = 6.5 MeV in ^{236}U which exceeds the fission barrier B_f = 5.6 MeV. For thermal neutrons the excitation energy E* of the compound is $E^* = S_n > B_f$. The isotope ^{235}U is said to be "fissile".

In contrast, the most abundant U-isotope ^{238}U has the separation energy S_n = 4.8 MeV smaller than the barrier height B_f = 6.3 MeV. It is non-fissile. To induce fission the incoming neutron energy must be E_n > 1.5 MeV. The difference of the binding energies S_N for the two U-isotopes is due to pairing. The ^{235}U isotope has an odd number of neutrons but by neutron capture becomes even in neutron number. There is hence a gain in pairing energy with a large S_n for the isotope ^{236}U. On the other hand, ^{238}U has an even number of neutrons. Following neutron capture the isotope ^{239}U has an odd number of neutrons with a more loosely bound unpaired neutron and smaller S_n. However, the isotope ^{239}U decays by 2 sequential β^-decays to ^{239}Pu which is again fissile. Therefore ^{238}U is said to be "fertile".

2. Mass Distributions of Fragments

Neutron-induced fission has almost exclusively been studied with targets in the actinides. The actinides cover the range of elements from Actinium (Z = 89) up to Lawrencium (Z = 103). In the chart of nuclides they lie in an island of relative stability. There are however only 3 isotopes with lifetimes of $T_{½}$ 10^9 a or longer. But also these isotopes eventually decay by α-emission or spontaneous fission.

Fission of pre-actinides and post-actinides (superheavy elements) was investigated with light or heavy ions as projectiles or by Coulomb excitation. Valuable information has also come from photofission with photons produced by bremsstrahlung.

In each of the above mass regions of the chart of nuclides the fragments have characteristic properties. Notably their mass distributions are specific and therefore of prime interest.

Discovering fission Otto Hahn proved the existence of Ba in U-samples irradiated by neutrons. From fission of Uranium the complement to Ba with Z = 56 is Kr with Z = 36. This asymmetry in charge or mass splits was later shown to be a general feature in the actinides, both for (n,f) reactions and spontaneous fission. This is shown in Fig. 5.

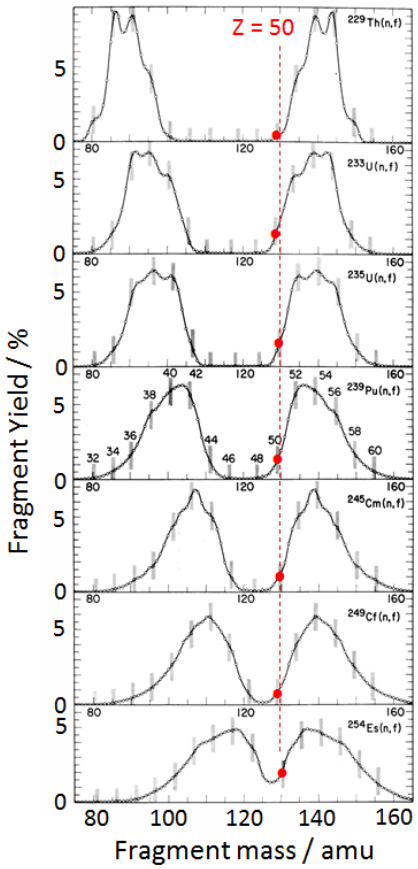

Fig. 5: Asymmetric fission in thermal neutron fission from Th(n,f) to Es(n,f). Adapted from [2]

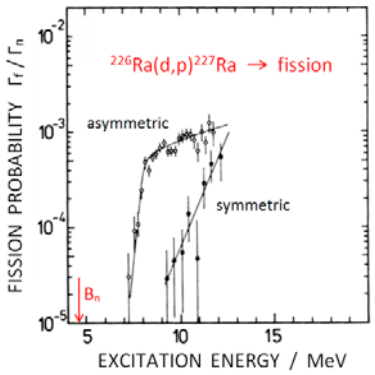

Fig. 6: Asymmetric fission of ^{227}Ra. Adapted from [3]

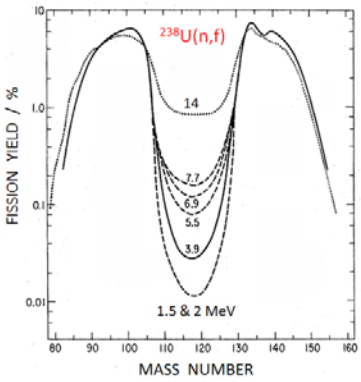

Fig. 7: Symmetric fission catching up with increasing excitation energy, Adapted from [4]

The asymmetric mass split in (n,f) reactions induced by thermal neutrons in targets from ^{229}Th to ^{254}Es has two remarkable features:

1) For all reactions the yields start rising in the heavy mass group at $A_H \approx 130$ u. The corresponding charge is the magic Z = 50. The mass center of the heavy group stays about constant, the mass center of the light group follows the increase of compound mass.
2) The mass yield curve exhibits a fine structure. It appears to be linked to even charge splits for the compound nuclei Th-Cf with even compound charges Z = 90 - 98.

In Fig. 6 the asymmetric and symmetric components of the mass distribution in the reaction ^{226}Ra(d,p)^{227}Ra are displayed as a function of excitation energy of the fissioning nucleus. The two types of fission, we may call them modes, behave differently. Apparently the asymmetric mode has a lower fission barrier compared to the symmetric mode.

A similar conclusion may be drawn in Fig. 7 for the reaction ^{238}U(n,f). At the threshold energy for incoming neutrons of 1.5 MeV the mass distribution is almost purely asymmetric and only with increasing excitation energy the symmetric mode comes into view.

The suggestion from experiment to discuss mass distributions in terms of two distinct modes, symmetric and asymmetric, is corroborated by theory. Calculations of the potential energy surface near the saddle point by different approaches clearly show the existence of two barriers, a lower asymmetric barrier and a higher symmetric barrier. This is shown in Fig. 8.

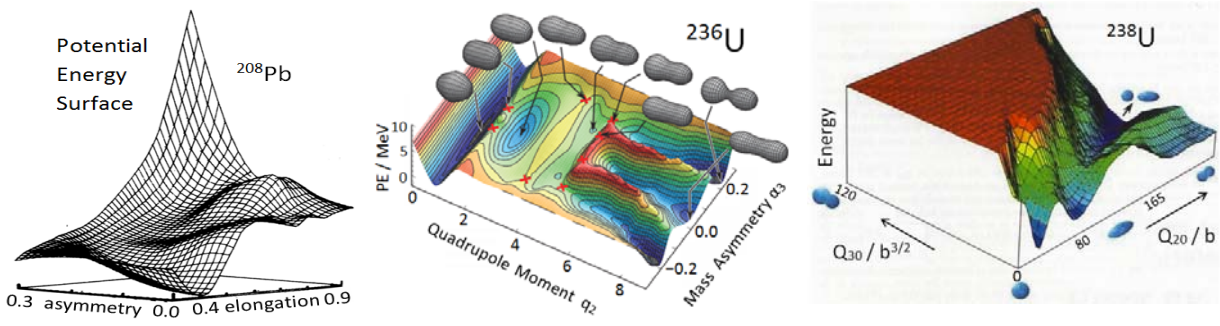

Fig. 8: To the left: shell corrected LDM model for ^{208}Pb (adapted from [5]). In the middle: shell corrected LDM model for ^{236}U (adapted from [6]). To the right: Microscopic HFB model for ^{238}U (adapted from [7]).

In the middle panel symmetric and asymmetric modes are seen to proceed along valleys towards scission. The two valleys are well separated by high ridges preventing a spillover from valley to valley. The two modes are in fact distinct and evolve independently. This is corroborated by experiment.

In the symmetric LDM mode no shell effects of fragments come into play while in the asymmetric mode the magic heavy fragment ^{132}Sn not only fixes the position of the heavy mass group but being spherical also favors more compact scission configurations. The kinetic energy of fragments is hence expected to be larger in the asymmetric mode than in the symmetric mode. The clean separation between the two modes becomes therefore better evident for mass distributions constrained by fragment kinetic energy. As visualized in Fig. 9 for ^{232}Th(n,f), the symmetric mode starts at mass symmetry with the total kinetic energy TKE = 160 MeV. Moving towards mass asymmetry the mode tapers off in yield but TKE stays constant. The

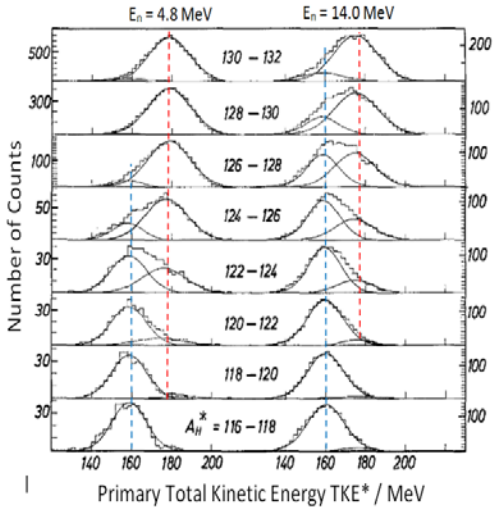

Fig. 9: Mass distribution from ^{232}Th(n,f) constrained by kinetic energy . Adapted from [8].

asymmetric mode comes into view already close to symmetric fission albeit at very small yield and in any case with TKE shifted to larger energies by some 20 MeV. In mass regions where one of the modes is prevailing the distribution of TKE is well described by Gaussians. However, in the mass ranges of mode overlap the TKE distribution is skewed. At lower TKE there is a tail first to the right, and for higher TKE to the left until the symmetric mode no longer contributes. The phenomenon was studied for two different incoming neutron energies E_n. It directly proves that there are as predicted by theory two distinct valleys leading from two saddle points differing in height to scission.

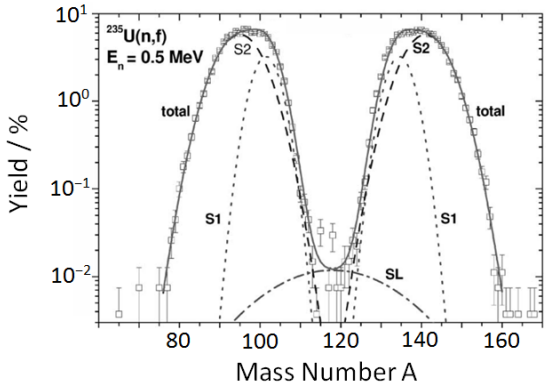

Fig. 10: Brosa modes in ^{235}U(n,f). Experimental data from IRMM. Adapted from [9]

In the detailed analysis of many fission reactions it turned out that a satisfactory description of mass and energy distributions requires the introduction of more than one mass asymmetric mode. By theory this was proposed in the Brosa-Grossmann-Müller model of scission [10]. The modes called for short the **Brosa modes** are the superlong symmetric mode (SL) and two asymmetric modes standard I and standard II (St I and St II). The bifurcation of the asymmetric mode into St I and St II occurs once the asymmetric saddle point has been passed. The position of the mode St I is centered at the heavy mass $A_H \approx 135$ while for the mode St II the center is at $A_H \approx 142$. It is therefore conjectured that St I is steered by the doubly magic ^{132}Sn and St II by the deformed neutron shell with N = 88. Note that for all three modes the mass distribution is assumed to be Gaussian in shape. In the example shown for the reaction ^{235}U(n,f) the fit is seen to be very satisfactory.

The combined analysis of mass and TKE distributions for ^{235}U(n,f) in terms of modes is convincing. Not only the mass distribution but also properties of the total kinetic energy TKE are consistently parameterized. The average <TKE> as a function of mass A is seen in Fig.11 to come about as a superposition of the three modes with each mode having its own characteristic TKE depending on mass. The weights of the modes are obtained from the fit to the mass distribution. Remarkably the variance σ_{TKE} of the TKE(A) distributions exhibits bumps at the overlap of modes.

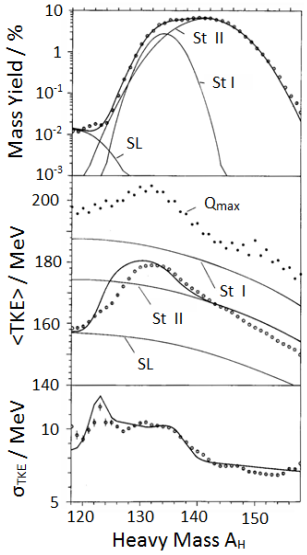

Fig. 11: Combined analysis of mass and energy in terms of Brosa modes. Adapted from [11].

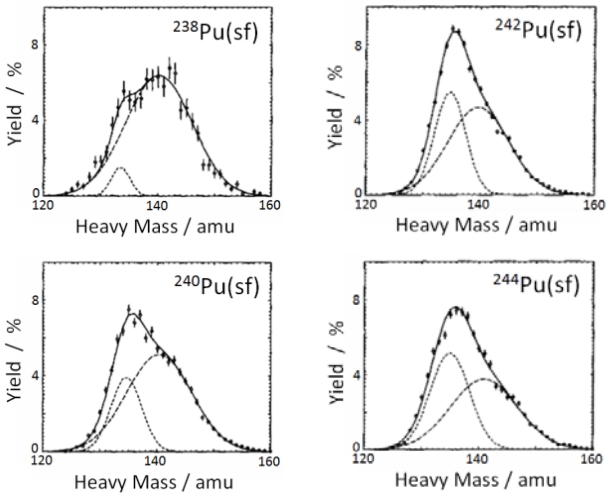

Fig. 12: Standard I and II modes in spontaneous fission of Pu-isotopes. Adapted from [12]

In the mass distributions of Pu-isotopes undergoing spontaneous fission a striking variation in the shape of the mass distributions is reported. The experimental data are given in Fig. 12. In the decomposition of mass yield into the modes Standard I and II it appears that the variation in shape should be attributed to varying weights of the two modes. Surprisingly the relative weights of the modes StI and StII change suddenly from isotope to isotope. It indicates that even having passed the barrier, the Potential Energy Surface in the descent from saddle to scission has a structure being very sensitive to the nucleon composition of the fissioning nucleus.

Exploring fragment mass distributions at very asymmetric splits of the fissioning nucleus a new phenomenon emerges. Comparing the mass distributions for ^{235}U(n,f) and ^{249}Cf(n,f) as visualized in Fig. 13 it is

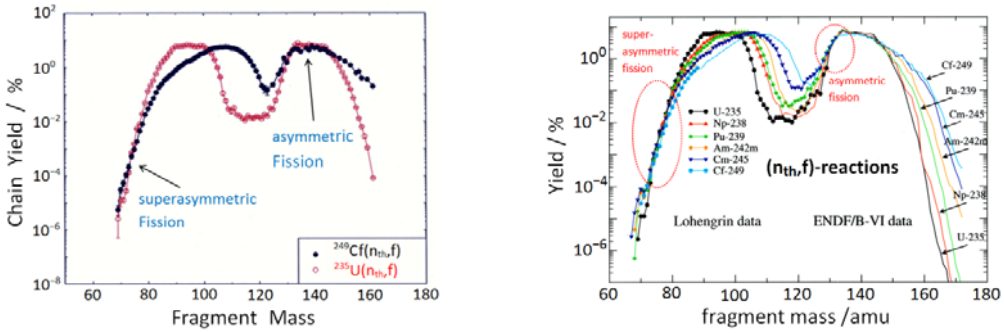

Fig. 13: Asymmetric and superasymmetric fission in thermal neutron induced fission of actinides

noticed that there are two mass regions where yields become virtually identical. Besides modes St I and St II stabilizing the asymmetric heavy peak by shell effects there exists at light masses near 70-80 amu a

further mass-range where yields are identical. This is attributed to the presence of shells with Z = 28 and N = 50 for ^{78}Ni in the light fragment. This coincidence of yields in the light fragment group is called **superasymmetric fission.** As shown in the right panel of Fig. 13 superasymmetric fission is observed in all thermal neutron reactions analyzed at the Lohengrin spectrometer of the Institut Laue-Langevin.

More in detail, superasymmetric fission in (n_{th},f) of ^{245}Cm in Fig. 14 (left panel) becomes manifest as a bump near A = 70 attributed to the high yield of ^{70}Ni with Z = 28. This bump has been found for all (n_{th},f) reactions studied. Less spectacular is a kink at mass A = 80 in the slopes of the mass distributions in Fig. 13 (right panel). Tentatively one may trace it to the stabilizing effect of ^{82}Ge with the magic neutron number N = 50 which after evaporation of 2 neutrons is observed as ^{80}Ge at mass A = 80.

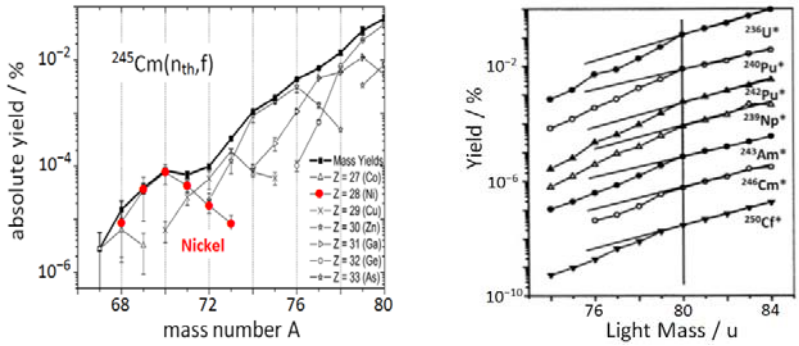

Fig, 14: Left panel: bump in the superasymmetric yield of ^{245}Cm(n,f) identified as increased yield of Ni with the magic proton number Z = 28. Adapted from [13]. Right panel: Kink at mass A = 80 at the border between standard asymmetric and superasymmetric fission. Adapted from [14].

In the potential energy surfaces near the barrier in Fig. 8 it becomes not evident that for the actinides there is a fine structure: the barriers are double-humped. This surprising feature emerges when both, tri-axial and asymmetric deformations of the nucleus on its way to scission are taken into account. Thereby the first hump is tri-axial while the second hump is axially symmetric but the dumb bell is asymmetric, i.e. the two ends have different size. A much discussed consequence of the double-humped structure is shape isomerism. When the nucleus populates states in the second minimum between the humps, the nucleus may stay there for some time before tunneling through the second barrier. Shape isomerism is not further discussed here.

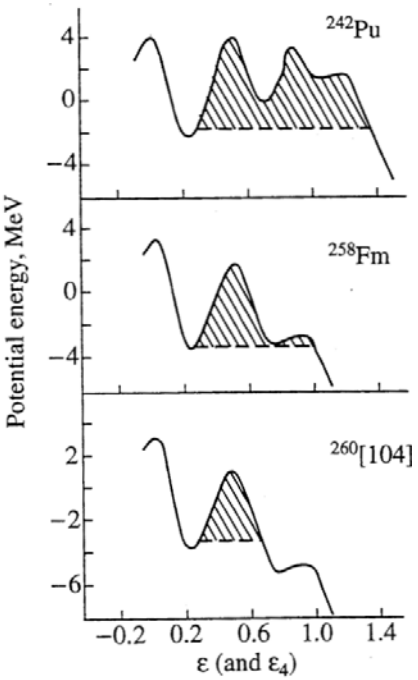

Fig. 15: Barrier shapes [15]

As concerns the symmetry-asymmetry character of mass distributions, it is the asymmetry of the second barrier which is considered to be the flash point for mass asymmetry in the actinides. The conjecture is confirmed by the fact that ^{258}Fm is the lightest isotope where the second barrier becomes negligible and where a transition from asymmetric to symmetric fission is observed. In Fig. 15 the hatched part of the barrier has to be tunneled when starting from the ground of the nucleus in the first minimum of the PES. Symmetric mass distributions obtain from mass A ≈ 256 to mass A ≈ 276 in the superheavies. The interesting phenomenon of **bimodal fission** appears in this mass range with two modes both symmetric in mass but with widely differing kinetic fragment energies.

3. Energy Distributions of Fragments

The energy available in n-induced fission is the Q-value:

$$Q^* = M_{Target} + M_{neutron} + E_{neutron} - (M_L^* + M_H^*) \quad (7)$$

It is shared between the total kinetic and the excitation energy TKE* and TXE, respectively, of primary fragments

$$Q^* = TKE^* + TXE. \quad (8)$$

To the total kinetic energy TKE* contribute both the light and the heavy fragment with their kinetic energies E_L^* and E_H^*:

$$TKE^* = E_L^* + E_H^* = (k/2)M_{CN}V_L^*V_H^*. \quad (9)$$

The total kinetic energy release is found by measuring fragment velocities V_L^* and V_H^* for given compound mass M_{CN} of the fissioning nucleus. The factor k = 1.0365 keeps track of the transformation of units to those in use in nuclear physics, *viz.* u for masses M, (cm/s) for velocities and MeV for energies.

In the CM system of fragments the momenta $\mathbf{p}_L^*$ and $\mathbf{p}_H^*$ of primary fragments cancel each other. The absolute values are equal:

$$M_L^*V_L^* = M_H^*V_H^* \quad \text{whence} \quad M_L^*/M_H^* = E_H^*/E_L^* \quad (10)$$

For the three standard reactions in thermal neutron fission ^{233}U, ^{235}U and ^{239}Pu the distributions of velocities P(V*) and kinetic energies P(E*) are compared in Fig. 16:

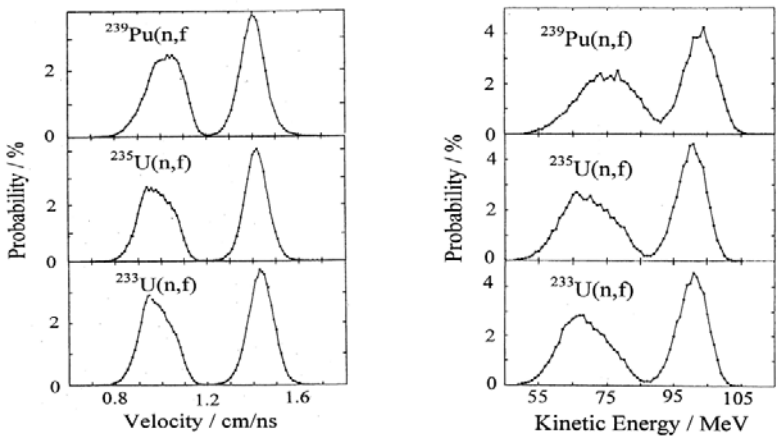

Fig. 16: Velocity and Kinetic Energy distributions for thermal neutron fission of ^{239}Pu, ^{235}U and ^{233}U. [16].

Evidently the two bumps to the left and right in the velocities and energies reflect the heavy and light mass group of fragments. Note that on average the velocity and energy for the light group is larger than for the heavy group.

Average velocities in cm/s, masses in amu and energies for the L and H group in MeV for the reaction ^{235}U(n_{th},f) are given in the table:

$\langle V_L^* \rangle$	$\langle V_H^* \rangle$	$\langle M_L^* \rangle$	$\langle M_H^* \rangle$	$\langle E_{KL}^* \rangle$	$\langle E_{KH}^* \rangle$
1.420(5)	0.983(5)	96.4(2)	139.6(2)	100.6(5)	69.8(5)

In the following table average total kinetic energies <TKE*> for thermal neutron and spontaneous fission are summarized:

Reaction	233U(n,f)	235U(n,f)	239Pu(n,f)	252Cf(sf)
TKE*/MeV	170.1(5)	170.5(5)	177.9(5)	184.0(13)

From the table it is noticed that the energy release increases with the mass or charge of the fissioning nucleus. From a fit to experimental data Viola proposed a dependence on the Coulomb parameter $Z^2/A^{1/3}$. The approach is very successful:

$$<TKE^*> = 0.1189(11)\, Z^2/A^{1/3} + 7.30(15)\ \text{MeV} \qquad (11)$$

Besides the average also the distribution of TKE* is of interest. Example: for ^{252}Cf(sf) it is Gaussian-like (left figure). In the figure to right the width of the distribution as described by the variance σ_{EK}^2 is seen to increase with fissility Z^2/A.

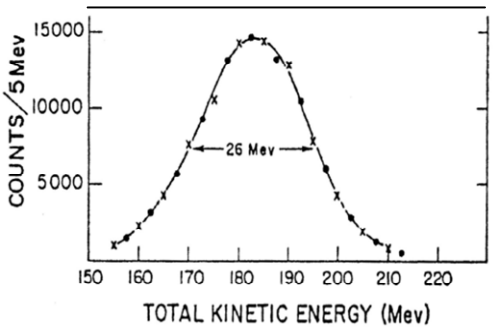

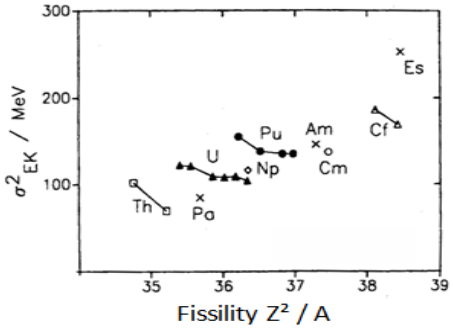

Fig. 17: Width of TKE in ^{252}Cf(sf). [17] Fig. 18: Variance versus fissility in (n_{th},f) reactions.[18]

Velocities and energies of fragments are in experiment a very common tool to determine fragment masses. The method is based on momentum and mass conservation:

$$M_L^*V_L^* = M_H^*V_H^* \quad \text{and} \quad M_L^* + M_H^* = M_{CN}\,.$$

The asterisk labels quantities before neutron emission. Since $E_L^*/E_H^* = V_L^*/V_H^*$ one finds both in double- velocity and double-energy measurements on complementary fragments L and H

$$M_L^* = M_{CN}[V_H^*/(V_H^*+V_L^*) \quad \text{and} \quad M_L^* = M_{CN}[E_H^*/(E_H^*+E^*)].$$

There is however a difficulty. Neutron emission is very fast. All neutrons are evaporated in times $<10^{-14}$ s. In experiment therefore always fragments after neutron emission are observed. The above equations can hence not be applied without corrections for neutron emission. For velocity measurement this task is simplified by the fact that due to the isotropic evaporation of neutrons from fragments the velocities remain on average unchanged: $V_{L,H} = <V_{L,H}^*>$. This means that to good approximation in 2V experiments average primary fragment masses are found. In 2E experiments neutron emission must explicitly be taken into account.

Besides kinetic energy the excitation energies of fragments are important to study. In principle the total excitation energy TXE could be found from energy conservation as

$$TXE = Q^* - TKE^*. \qquad (12)$$

However, to calculate Q* not only the primary mass distributions Y(A*) but more in detail the yields Y (A*,Z) have to be known. This is unfortunately not the case and therefore TXE has to be found by adding its contributions to n and γ emission:

$$TXE = E_{ntot} + E_{\gamma tot} = \nu_{tot}\cdot [B_n + \eta] + E_{\gamma tot} \qquad (13)$$

with ν_{tot} the total neutron multiplicity, B_n the neutron binding energy, η the neutron kinetic energy in the CM system of fragments and $E_{\gamma tot}$ the total prompt gamma energy. The average total excitation

energy <TXE> calculated for thermal neutron and spontaneous fission in a range if actinides is presented in Fig. 19:

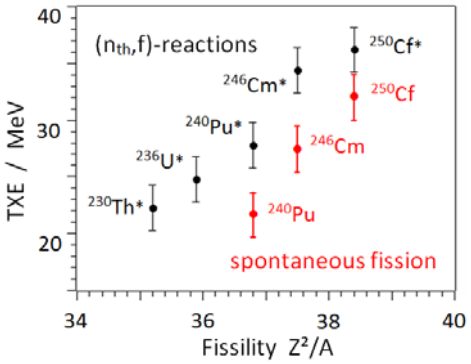

Fig. 19: Total excitation energy for thermal neutron and spontaneous fission in the actinides

There is a clear correlation between the excitation energy <TXE> and the fissility parameter Z^2/A. The increase of <TXE> with fissility follows the increasing neutron emission for heavier nuclei. As a rule, in spontaneous fission average excitation energies <TXE> are smaller than in thermal neutron fission. This may be attributed to the smaller potential energy gain ΔV from the exit point of the barrier down to scission in spontaneous fission.

Both energies, total kinetic energy TKE* and total excitation energy TXE, are already present at the scission point with a certain fraction. However, major contributions are at scission still bound as potential energies V_{Coul} and V_{def} respectively. Formally

$$TKE^* = E_K^{sci} + V_{Coul} \quad \text{and} \quad TXE = E_X^{sci} + V_{def} \tag{14}$$

V_{Coul} is the energy of mutual Coulomb interaction between fragments, and V_{def} the deformation energy of the two fragments at the scission point. The energies at scission E_K^{sci} and E_X^{sci} not bound as potential energies are fed by the gain in potential energy ΔV in the descent from saddle to scission and the excitation energy of the compound nucleus E_{CN}^* left at the barrier B_f:

$$E_K^{sci} + E_X^{sci} = \Delta V + (E_{CN}^* - B_f) \tag{15}$$

The share of E_K^{sci} and E_X^{sci} in the potential energy gain ΔV is discussed controversially. It depends on the viscosity of the flow of nuclear matter from saddle to scission. Is the flow honey- or water-like? In experiment the dissipated energy E_X^{sci} has been estimated from the charge even-odd effect of fragments. Combined with theoretical models for the energy gains ΔV the pre-scission energy E_X^{sci} is derived albeit with large uncertainties as $E_X^{sci} = \Delta V - E_K^{sci}$. In fig. 20 the estimation based on a model for the charge even-odd effect is indicated by stars in near-barrier fission. The through-going line is a fit to these data in a two-spheroid model (TSM). Further data sets are from purely theoretical models (Bonasera and Wilkins).

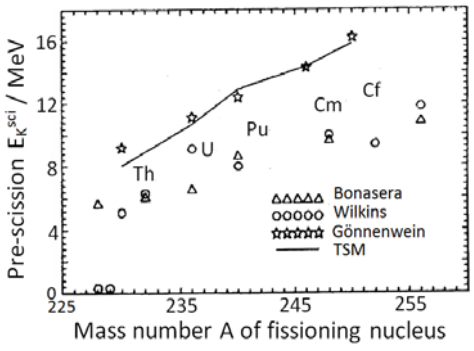

Fig. 20: Pre-scission kinetic energy *versus* mass number of fissioning nucleus [19].

Finally the correlation between mass and energy of fragments has to be inspected. These correlations were investigated in a series of classic papers setting standards when surface barrier diodes became available as convenient detectors for heavy ions. The main reactions being of importance for applications were studied in the sixties of last century. Mass distributions before and after prompt neutron emission, Y(M*) and Y(M), respectively, average pre-neutron kinetic energies of single fragments $<E_K^*(M^*)>$ as a function of mass M*, total average kinetic energies <TKE*(M*)> and variances $\sigma_{EK}(M^*)$ of energy were

surveyed. The results obtained for the reaction $^{235}U(n_{th},f)$ are on display in Fig. 21. Notable facts are:

- mass distributions of both, primary fragments Y(M*) and secondary fragments Y(M)have fine structure with a spectacular spike for M = 134 in Y(M)
- light fragments have large kinetic energies staying virtually constant throughout the mass group
- the total kinetic energy TKE* is largest for the mass M* = 132
- Dip in kinetic energy near mass symmetry
- the variance exhibits structure when modes overlap as already pointed out in Fig. 11

Results shown here for $^{235}U(n_{th},f)$are similarly found for thermal neutron induced fission of ^{233}U and ^{239}Pu, and spontaneous fission of ^{252}Cf. They are typical in low energy fission of actinides

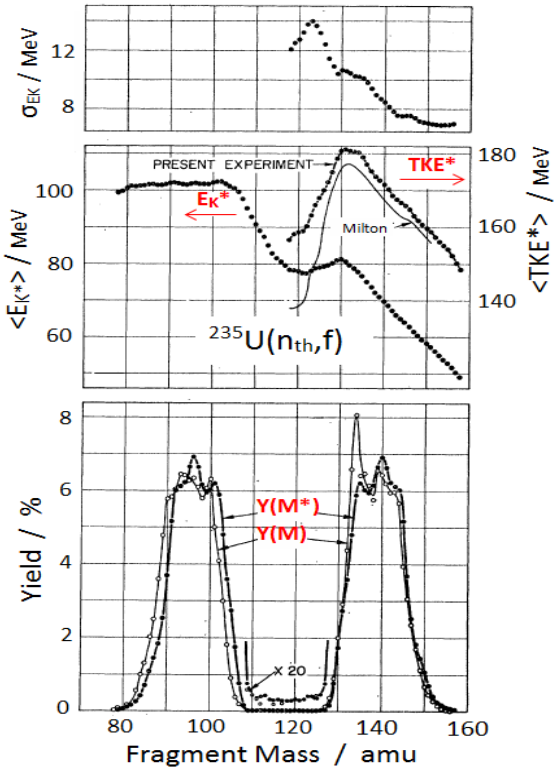

Fig. 21: Reaction $^{235}U(n_{th},f)$: pre- and post-neutron mass distributions Y(M*) and Y(M) ; fragment and total kinetic energy $<E_K^*>$ and $<TKE^*>$ as a function of fragment mass; variance σ_{EK} as a function of fragment mass. [20].

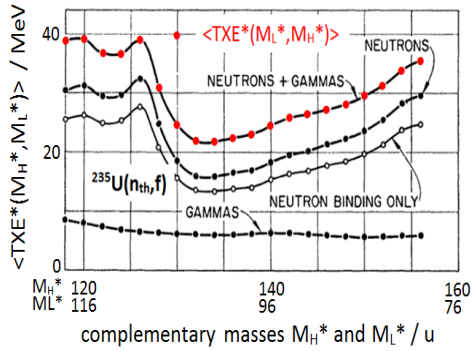

It is instructive to compare mass by mass the kinetic and excitation energies of fragments. Complementary to Fig. 21, in Fig. 22 the total excitation energy <TXE> of complentary masses is on display for the reaction $^{235}U(n_{th}.f)$. It is evaluated according to eq. (13) as the sum of contributions by neutrons and gammas. As to be expected from energy conservation, the dip in kinetic energy is compensated by a large excitation energy.

Fig. 22: Total excitation energy *versus* fragment mass. [20]

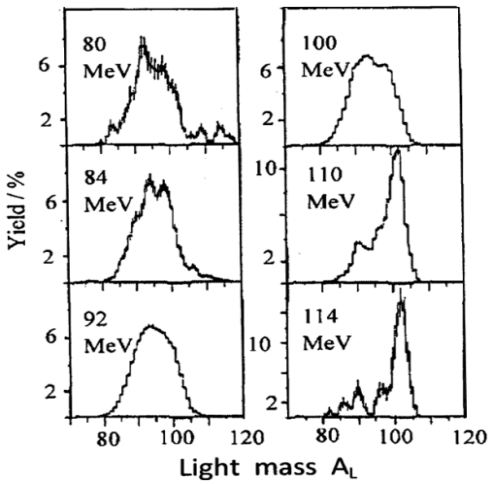

The fine structure of mass distribution has also been studied for narrow windows of kinetic energy. The structures are found to vary rapidly with energy. Samples of mass distributions for $^{235}U(n_{th},f)$ within energy windows of ΔE_L = 4 MeV in width for the light group are only Gaussian-like for energies near the average. Both at very high and at very low energies a fine structure appears with peaks about 5 mass units apart. The phenomenon has been scrutinized in connection with fragment charge even-odd effects in cold fission. It has prompted the notions of cold compact and cold deformed fission at high and low kinetic energies.

Fig. 23: Mass distributions in narrow windows of E_L [21]

4. Charge Distributions of Fragments

Charge distributions of fission fragments closely follow the mass distributions. The ratio of fragment charge numbers to mass numbers Z_{FF}/A_{FF} is to first approximation identical to the corresponding ratio Z_{CN}/A_{CN} of the fissioning compound nucleus. There are only slight deviations from this UCD rule of "unchanged charge density". Note that $Z_L + Z_H = Z_{CN}$.

However, in particular in low energy fission of actinides, there is a pronounced staggering of charge yields Y(Z) in case of even-Z fissioning compounds. The phenomenon has been scrutinized by radiochemical and physical methods for reactions ranging from (sf), (n,f), (γ,f) … to fission by Coulomb excitation. In the following mainly n-induced fission is considered.

Comprehensive studies were performed at the Institut Laue-Langevin for the (n,f) reaction with thermal neutrons for targets from ^{229}Th to ^{249}Cf. A sample of charge distributions measured for even-Z compounds is shown in the Fig. 24. Only results for the light fragment group are given. For e-Z compounds the charge yields in the heavy group are strictly identical to those in the light group mirrored

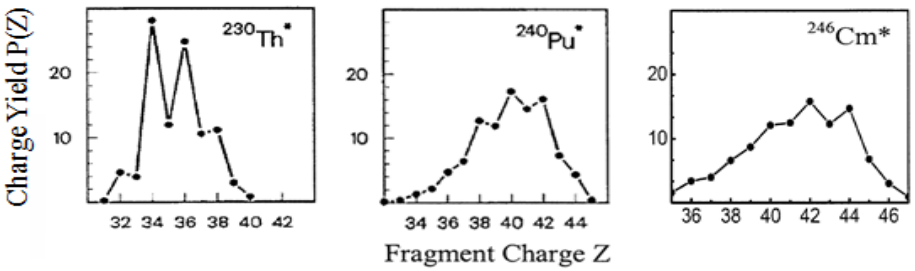

Fig. 24: Charge distributions in the light mass group of e-Z compounds in (n_{th},f) reactions. [22]

at symmetry. Since upon approaching symmetric fission the charge yields in the figure are seen to fade away, the full charge distributions are like the mass distributions asymmetric.

Catching the eye in the figure is the strong even-odd fluctuation in the charge yields. Systematically even fragment charges are favored compared to odd ones. The effect is most noticeable in the light actinide Th and nearly vanishes for the heavier actinide Cm. The question then is whether this tendency has to be attributed to the increase of compound mass A_{CN}, or compound charge Z_{CN}, or fissility Z_{CN}^2/A_{CN}, or any other parameter. An answer to this question may be found by inspecting charge distributions for

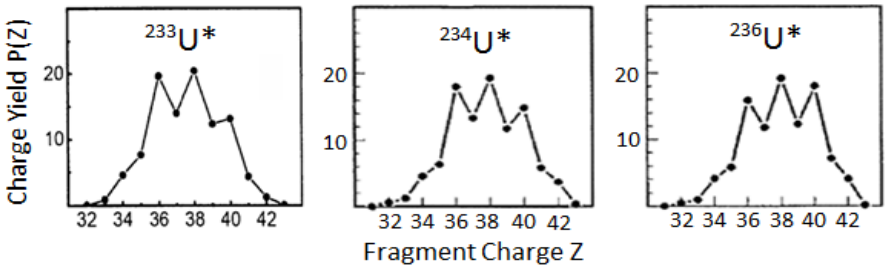

Fig. 25: Charge distributions for the isotopes ^{233}U, ^{235}U and ^{236}U in (n_{th},f) [22].

fixed charge Z_{CN}. This is done in Fig. 25 for three U-isotopes with $Z_{CN} = 92$. The staggering is observed to stay pretty constant. It is hence concluded that the e-o staggering depends crucially on compound charge Z_{CN}. The compound neutron number N_{CN} or mass number A_{CN} does not appear to influence the effect.

The even-odd staggering was also analyzed for neutrons. There is however a difficulty due to the evaporation of neutrons from the fragments. Except for cold fission with no neutron emission at all, a strict conservation law $N_{LF}^* + N_{HF}^* = N_{CN}$ is only valid for primary fragments before neutron emission. Yet, the simultaneous measurement of primary masses A_{FF}^* and charges Z_{FF} is in practice not feasible.

Starting from the idea that the e-o staggering of charge yields in fission of even-Z_{CN} compound nuclei is a reminiscence of the superfluid fully paired ground state of e-Z nuclei, it was conjectured that for odd-Z_{CN} nuclei with an unpaired proton any e-o fluctuation in charge yields should be absent. For the odd-Z_{CN} nuclei Np and Am this was indeed observed in standard asymmetric fission as shown in Fig. 26. However, surprises came when moving to super-asymmetric fission as discussed below.

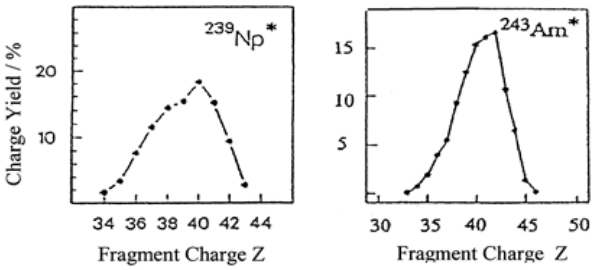

Fig. 26: Charge distributions in the light mass group of the compound nuclei ^{239}Np* and ^{243}Am* [23].

Knowing masses and charges of fission fragments allows for a more detailed insight into the distributions of fragments. Two types of conditional distributions may be evaluated:

isotopic mass distributions **Y(A|Z)** and isobaric charge distributions **Y(Z|A).**

How these distributions are defined and found is visualized in a zoom of the nuclide chart.

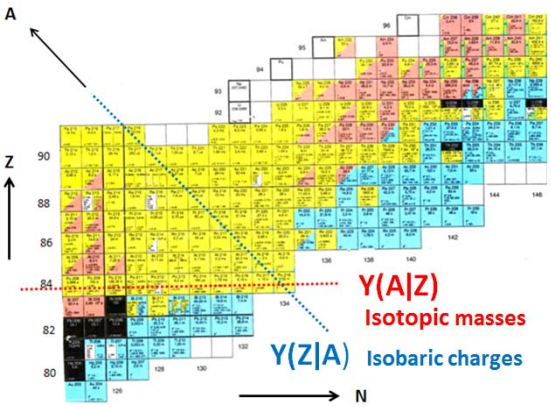

Fig. 27: Isotopic mass distribution Y(A|Z) and isobaric charge distribution

In particular the isotopic mass distributions are often referred to because they demonstrate directly the relation between fine structure in the mass yields and the even-odd staggering of charge yields. For the reaction ^{235}U(n,f) with thermal neutrons the individual isotopic mass distributions Y(A|Z) together with their sum, the mass distribution Y(A), are plotted for the light fragment group in Fig. 28. Evidently the large yields of isotopic mass distributions for even fragment charges Z_L bring about the fine structure in the mass yield Y(A). The bumps in Y(A) are about 5 u apart just corresponding to a step of two charges. The 3D plot in Fig. 29 for ^{232}U(n_{th},f) with projections of the isotopic distributions Y(A|Z) on the A-plane and the Z-plane makes understandable how a strong fluctuation in charge yields leads to gentle modulations of the mass yield.

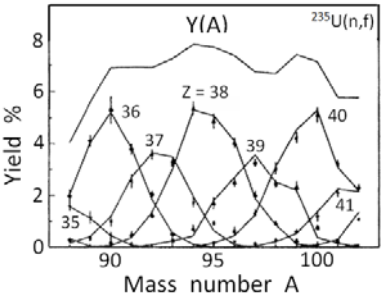

Fig. 28 to the left: Mass yield Y(A) of ^{235}U(n,f) and the underlying isotopic distribution Y(A|Z). [24]

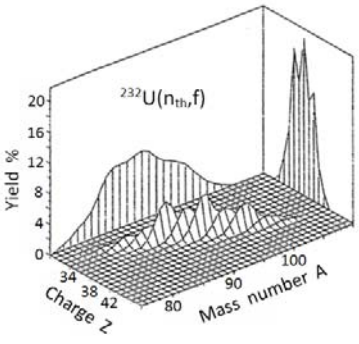

Fig. 29 to the right: 3D plot for ^{232}U(n,f) of isotopic distributions Y(A|Z) and their projections as mass yield Y(A) and charge yield Y(Z). [25]

The most discussed feature of charge distribution is the conspicuous even-odd staggering of their yields. To quantitatively assess the fluctuations of charge yields in fission the even-odd effect δ_Z is introduced with the definition

$$\delta_Z = (Y_e - Y_o) / (Y_e + Y_0). \qquad (16)$$

In this definition Y_e and Y_0 are the sum of yields for even and odd charges, respectively. It is common use to normalize the sum to $(Y_e + Y_0) = 100$ and to quote the e-o effect δ_Z in %.

In the table e-o effects for thermal neutron fission have been collected. Except for ^{238}Pu*studied by radiochemistry, the data were obtained by physical methods at the ILL. The obvious decrease of the

Nucleus	^{230}Th*	^{233}U*	^{234}U*	^{236}U*	^{239}Pu*	^{240}Pu*	^{242}Pu*	^{246}Cm*	^{250}Cf*
δ_Z / %	41.2(10)	20.3(15)	22.1(21)	23.4(10)	13.3(40)	11.7(5)	10.0(15)	9.3(12)	4.6(7)

e-o effect when moving through the actinides was already addressed in connection with Fig. 24. There it was also argued that the effect essentially depends on the compound charge Z_{CN} but not on compound mass A_{CN}. This is brought to evidence in two figures for δ_Z as a function of compound mass and compound charge. For the three U- and the three Pu-isotopes the e-o effect is constant telling that the effect does not depend on the neutron number N_{CN} of the compound. By contrast, in a logarithmic plot of the e-o effect versus compound charge Z_{CN}, the effect is a smooth linear function sloping down for increasing charge.

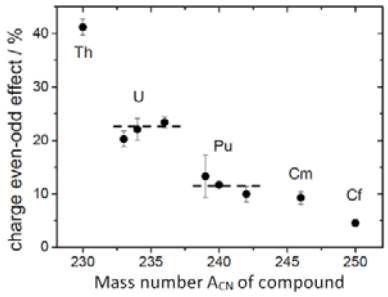

FIG. 30 to the left: Charge e-o effect *versus* compound mass, From [25]

Fig.31 to the right: Charge e-o effect *versus* compound charge. From [25]

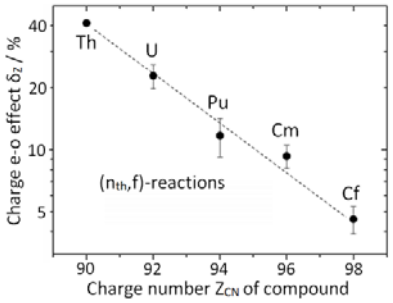

There is an interesting interpretation of the charge e-o effect. In thermal neutron fission of fissile nuclei the nucleus is cold and hence fully paired at the saddle. The appearance of odd fragment charges indicates that in the process of fission proton pairs are broken. The energy required has to be provided by the excitation energy E_X^{sci} the nucleus already has at the saddle or is gaining in the descent from saddle to scission. The more excitation energy is available, the more pairs may be broken and the more the e-o effect is washed out. A first hint to support this idea is found in a plot of δ_Z *vs.* total TXE from Fig. 19. This is on display in Fig.32. A clear correlation is revealed. Since TXE = E_X^{sci} + V_{def} it seems likely that the correlation is due to E_X^{sci} being responsible for the breaking of proton pairs.

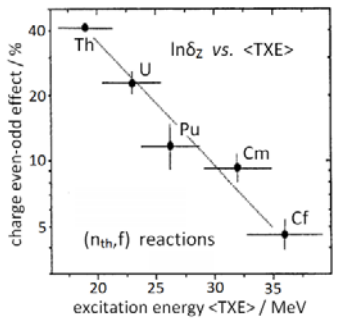

Fig. 32 to the left: Charge e-o effect *versus* total excitation energy. From [25]

Fig. 33 to the right: Charge e-o effect *versus* excitation energy at saddle. From [22].

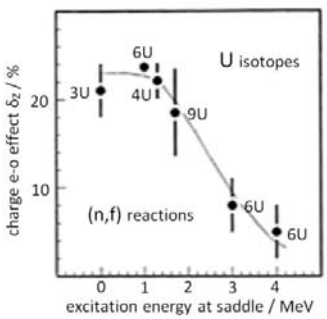

A cleaner argument is provided from a study of the charge e-o effect for ^{233}U, ^{234}U and ^{236}U at various excitation energies above the saddle. Any excitation energy at the saddle will go into excitation at scission.

As to be seen in Fig. 33, experiment clearly demonstrates the dependence of the charge e-o effect on the excitation at the saddle and hence contributing to the excitation at scission. The charge e-o effect is thus a sensitive detector of excitation energy at scission.

Several theories have been developed to find from the even-odd effect δ_Z observed in fission of even Z_{CN} compound nuclei the excitation energy at scission E_X^{sci}. It is remarked that for near-barrier fission the fissioning compound is superfluid at the saddle with all protons and neutrons being paired. The e-o effect $0 < \delta_Z < 1$ signals the presence of an odd number of protons in the fragments. It must come about by quasi-particle excitations breaking proton pairs in the course of fission from saddle to scission or right at scission provided the two single protons from a pair are going to complementary fragments. The mechanism of pair-breaking is left open.

Formally the following quantities are introduced:

N_{max} = maximum number of q-p excitations available depending on excitation energy E_X^{sci} at scission

q = probability to break a pair when the energy is available

ε = probability for broken pair to be a proton pair

p = probability for nucleons from a broken pair to go into complementary fragments.

With the normalization of charge yields $(Y_e + Y_o) = 1$ the e-o effect $\delta_Z = (Y_e - Y_o) / (Y_e + Y_o)$ becomes $\delta_Z = (1 - 2Y_o)$. If at most one pair only can be broken ($N_{max} = 1$) the odd charge yield Y_o of fragments is $Y_0 = q\varepsilon p$. Hence $\delta_Z = (1 - 2q\varepsilon p)$. For $N_{max} > 1$ it follows

$$\delta_Z = (1 - 2q\varepsilon p)^{Nmax}. \qquad (17)$$

On the other hand the energy consumed is given by the average number <N> of broken pairs with the energy 2Δ required to create 2 q-p excitations. Since $<N> = qN_{max}$ the excitation energy at scission is $E_X^{sci} = 2\Delta q N_{max}$. With eq. (17) the relation between the charge e-o effect and the excitation energy becomes

$$E_X^{sci} = \frac{}{} \ln\delta_Z \qquad (18)$$

The model outlined describes in physical terms the way how perfect superfluidity for near-barrier fission at the saddle point, is partially destroyed in the fragments. The model predicts that the excitation energy at scission E_X^{sci} is proportional to the logarithm of the e-o effect δ_Z.

The model does however not allow giving precise figures for the energy E_X^{sci} since the only parameter known with certainty is 2Δ = 1.7 MeV at the saddle point. For the parameter ε a reasonable approximation is $\varepsilon = Z_{CN} / ACN$. But the choice for the parameters q and p is pure guess work. To first approximation the two may be set as q = ½ and p = ½. With this choice one finds $E_X^{sci} = -3.8 \ln\delta_Z$.

Since according to the model the energy E_X^{sci} is proportional to the negative logarithm $-\ln\delta_Z$, and since δ_Z when plotted logarithmically decreases linearly with the compound charge number Z_{CN}, the energy drained up to scission from the potential energy gain ΔV increases linearly with compound charge Z. As visualized in Fig. 34, for thermal neutron fission of actinides from Th to Cf the energy E_K^{sci} increases from about 3 to 12 MeV. From Fig. 35 it appears that roughly ⅓ of the energy gain ΔV gain between saddle and scission is drained by excitation energy. The difference $(\Delta V - E_X^{sci})$ goes into kinetic energy at scission.

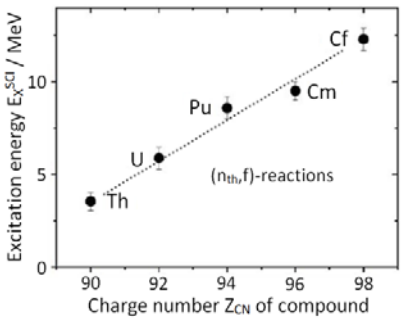

Fig. 34 to the left: Excitation energy at scission E_K^{sci} *versus* compound charge.

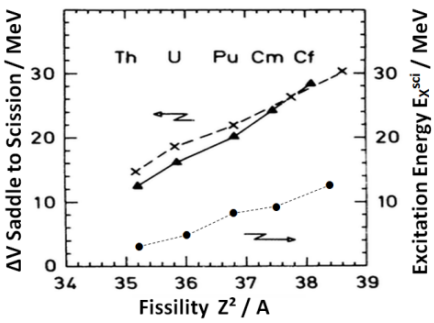

Fig. 35: Excitation energy E_K^{sci} and energy gain ΔV between saddle and scission, Crosses [26]. Triangles [27].

It has to be underlined once more that a rather large uncertainty remains as to the absolute size of the excitation and kinetic energies to be shared. Other choices of the parameters may be conceived. In case the breaking of proton pairs occurs only right at scission where deformations of fragments are large, the energy required for breaking 2ΔV is estimated to be larger by a factor . It is then also plausible that the two protons will go to complementary fragments which means p =1. Keeping to ε = 0.4 and q = 0.5 the excitation energy becomes $E_X^{sci} = -2.3 \ln\delta_Z$. By the way, this relation would better fit the dependence of the e-o effect as a function of the excitation energy at the saddle point measured in experiment.

Inspecting the charge distributions for even-Z compound nuclei it emerges that the e-o staggering is not constant over the full range of charges. This has been the motivation for introducing the notion of local e-o effects $\delta_Z(Z)$ depending on fragment charge Z. Various prescriptions how to assess this local e-o effect have been proposed.

In particular the local e-o effect highlights the rise of the e-o staggering of fragment charge yields in super-asymmetric fission. This is visualized in Fig. 36 for the light fragment group of $^{235}U(n_{th},f)$. The

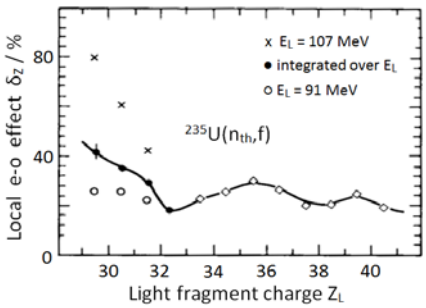

Fig. 36 to the left: Local e-o effect for two fixed fragment energies and integrated over energy E_L for $^{235}U(n_{th},f)$ [28]

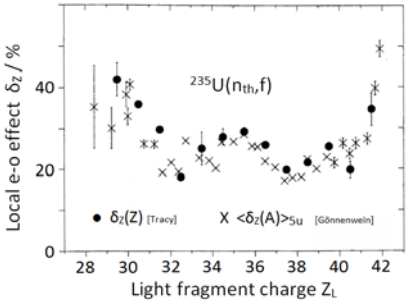

Fig. 37: Local e-o effect for $^{235}U(n_{th},f)$ evaluated by two different prescriptions [18]

local e-o effect is seen to steeply rise when approaching super-asymmetric fission for Z = 28 and N = 50 at large fragment kinetic energies E_L and hence low excitation energies.

The physical reason for the surge of e-o staggering is thought to be due to the shell effect in the light fragment. Magic fragments are not likely to pick up protons from a broken pair. For this conjecture to be valid a similar rise of the e-o staggering should also be observed close to the magic heavy fragment with Z_H = 50. This appears to be the case for $^{235}U(n_{th},f)$ where in Fig. 37 two different evaluations come to the result that for Z_L = 42 and hence Z_H = 50 e-o effects are enhanced.

As outlined in Fig. 26, in standard fission of compound nuclei with odd charge numbers Z_{CN} like Np with Z_{CN} = 93 there is no sizable e-o staggering . This is to be expected for a nucleus with a single un-paired proton which is free to move to one or the other fragment. But when in fission of nuclei with even Z_{CN} the large e-o effects became known, the measurements were also pushed for o-Z_{CN} into these mass regions of low yield. As shown for $^{238}Np(n_{th},f)$ the same surge of the even fragment charges was found. This result corroborates the interpretation given that in super-asymmetric fission the magic light fragment will not attract unpaired protons.

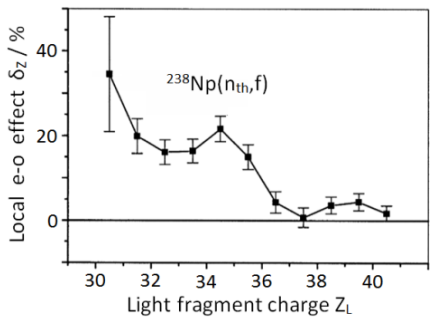

Fig. 38: Rise of the local e-o effect for the charge $\delta_Z(Z)$ in thermal neutron fission of the odd compound nucleus ^{239}Np in super-asymmetric fission [14].

It should finally be noted that in cold fission, where all available energy is getting exhausted by the total kinetic energy of fragments, completely new phenomena concerning e-o effects are showing up, both for protons and neutrons.

5. Neutrons and Gammas emitted from Fission Fragments

The energy balance in fission reads in eq. (8) Q* = TKE* + TXE with Q* the total available energy calculated from mass tables and TKE* the total kinetic energy of fragment determined by experiment. Though the main part of the available energy Q* is converted into kinetic energy TKE* a sizable fraction of excitation energy TXE remains. Average excitation energies <TXE> in thermal neutron induced and in spontaneous fission are presented in Fig.19. Typical examples are <TXE > ≈ 24 MeV for the reaction ^{235}U(n_{th},f) and <TXE> ≈ 36 MeV for spontaneous fission of ^{252}Cf. This energy is evacuated by the emission of neutrons and gammas as indicated in eq. (13).

Since evaporation times for neutrons are much shorter than emission times for gammas, excited fragments first cool down by neutron emission. Following neutron emission by "primary fragments" (labelled by an asterisk) the nuclei are called "secondary fragments" or simply "products". When the remaining excitation has fallen below neutron binding energies the emission of gammas is setting in. The change-over from neutron to gamma emission is at about 10^{-14} s. Gamma emission may last for several ms. Fission products reach their ground states by this γ-emission. Yet they are still too n-rich and hence unstable and liable to β^-–decay. The decay times may be very long. The radioactivity of fission products is part of the activity of fuel remnants from nuclear power stations.

Characteristic times for the different phases of the fission process are reviewed along with a scheme of the process in Fig. 39. The individual times are

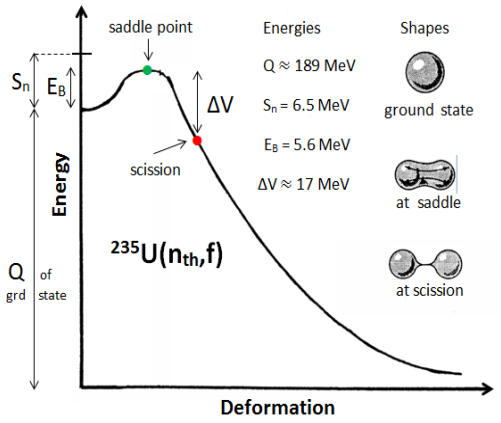

- From grd state to saddle in low energy fi: $6 \cdot 10^{-15}$ s
- From saddle to scission ≈ 5 zs
- Neck rupture in ≈ 0.5 zs
- Acceleration of FF to 90% of final velocity ≈ 5 zs
- Relaxation of deformation ≈ 5 zs
- Evaporation time for 10 MeV neutron ≈ 10^3 zs

Fig.39: Characteristic times in fission

Once the saddle has been passed the fission process is very fast, while it takes comparatively a long time to evaporate a neutron. This justifies the assumption that the bulk of neutrons is emitted from fully accelerated fragments.

The time scale of fragment de-excitation by neutrons and gammas is visualized in Fig. 40.

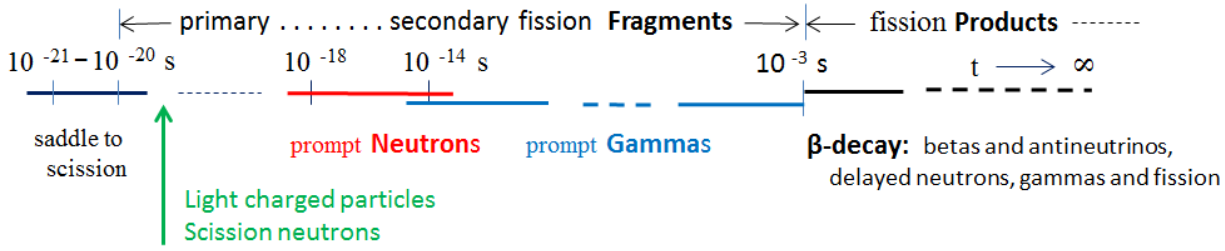

Fig. 40: Time scales in the de-excitation of fission fragment

5a. Neutrons

In low energy fission by far most neutrons are evaporated from fully accelerated fragments. They exhaust the main part of the excitation energy TXE of fragments. According to eq. (14), to TXE contribute the intrinsic excitation E_X^{sci} accumulated in the descent form saddle to scission and the energy stored as deformation energy V_{def} at scission but converted into intrinsic excitation once the deformation is relaxed after neck rupture. Eq. (14) is recalled for convenience:

$$TXE = E_X^{sci} + V_{def}. \qquad (14)$$

This energy is shared between neutrons and gammas with eq. (13) being recalled for convenience:

$$TXE = E_{ntot} + E_{\gamma tot} = \nu_{tot} \cdot [B_n + \eta] + E_{\gamma tot} \qquad (13)$$

with E_{ntot} and $E_{\gamma tot}$ the total neutron and gamma energies, ν_{tot} the total neutron multiplicity and B_n the neuron binding energy.

Neutron multiplicity ν_n is a key parameter of fission. It is defined as the number of neutrons emitted per fission event. The table gives some examples for the average multiplicity <ν> in thermal neutron fission of actinides:

CN nucleus	230Th	234U	236U	240Pu	246Cm	250Cf
$<\nu_{tot}>$	2.08	2.50	2.43	2.89	3.83	4.08

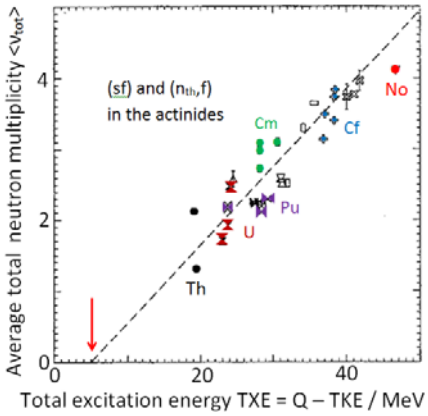

Neutron multiplicity is a reliable measure of the total energy of fragment excitation at scission. This is demonstrated in Fig. 41 where the average $<\nu_{tot}>$ is observed to increase linearly with excitation energy TXE. The offset marked by a red arrow in the figure is due to the energy not evacuated by neutrons but by gammas.

Fig. 41: Average total neutron multiplicity $<\nu_{tot}>$ total versus excitation energy TXE evaluated as (Q* − TKE*) for (sf) and (n_{th},f) in the actinides. Adapted from [29].

The distribution of total neutron emission numbers is Gaussian-like in low-energy fission (spontaneous fission, thermal neutron induced fission), with centers at the average neutron multiplicity <ν>. Very early in the history of fission research it was remarked that the Gaussians are universal, i.e. identical for all low energy fission reaction [30]. The standard deviation σ for all these reactions was given to be σ = 1.08.

$$P(\nu) = 0.36 \exp[-(\nu_{tot} - <\nu_{tot}>)^2 / 2\,\sigma^2] \quad \text{with } \sigma = 1.08 \qquad (19)$$

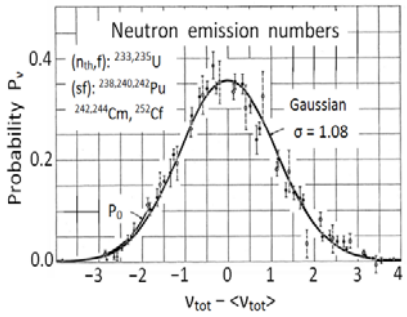

Fig. 42: Gaussian ν-distribution

Nowadays it is established that the above rule for P(ν) is oversimplified. Only for actinides from U to Cm the variance σ^2 is roughly constant with $\sigma^2 \approx 1.3$. For the actinides from Cf to No variances rise significantly.

Of particular interest are the probabilities P_0 for neutron-less fission with ν = 0. Compare (n_{th},f) of ^{235}U and (sf) of ^{252}Cf. Average multiplicities are <ν> = 2.43 and <ν> = 3.7. Though the averages <ν> are close together, the probabilities for neutron–less fission P_0 differ by a factor of 14: P_0 = 3.2 % and P_0= 0.23 %, respectively.

An important result from neutron studies in fission is the discovery that the neutron multiplicity has a peculiar dependence on fragment mass. Plotted as a function of fragment mass the average multiplicity <v(A)> has a saw-tooth like appearance. All experiments agree as to the general trends.

The neutron saw-tooth is best pronounced in low energy fission as demonstrated for ^{252}Cf(sf) and ^{235}U(n_{th},f) in the figures 43 and 44. Shown are the averages <v(A)> as a function of mass A.

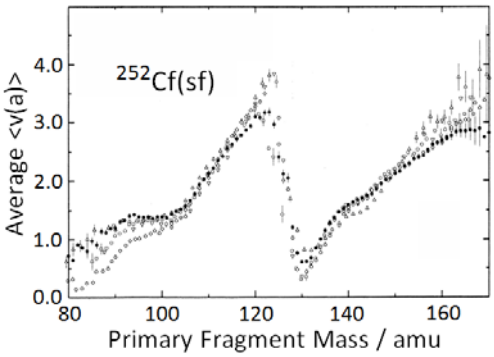

- Vorobyev 2001 [31]
- Signabieux 1972 [33]
- Budtz-Jörgensen 1988 [35]
- Zakarova 1979 [32]
- Walsh 1977 [34]

Fig. 43: Neutron distribution as a function of primary fragment mass for ^{252}Cf(sf)

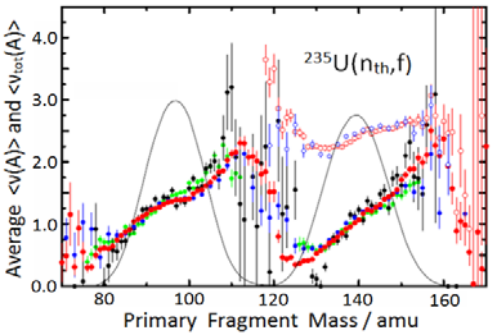

For <v(a)>

- Nishio 1998 [36]
- Müller 1984 [38]
- Maslin 1967 [37]
- Vorobyev 2009 [39]

For <v_{tot}(A)>

- Maslin 1967 [37]
- Vorobyev 2009 [39]

Fig. 44: Neutron distribution as a function of primary primary mass for ^{235}U(n_{th},f)

The saw-tooth phenomenon is intriguing. It is closely linked to the peculiarities observed in the mass-energy distributions of fragments. The minimum neutron multiplicity of <v(A)> for heavy fragment masses near A = 130 is the most startling feature. It is a further evidence for stiff magic fragments close to ^{132}Sn remaining un-deformed at scission and hence carrying no deformation energy V_{def} and only the comparatively small excitation energy E_X^{sci} at scission. All deformation energy is stored in the shape-distorted complementary light fragment. After shape relaxation the deformation energy is released by neutron evaporation leading to the peak in the saw-tooth of <v(A)>.

On average the light fragment group as a whole emits generally more neutrons than the heavy fragment group. Calling the group emission numbers v_L and v_H, respectively, some examples for v_L / v_H are collected in the table.

Reaction	^{233}U(n_{th},f)	^{235}U(n_{th},f)	^{252}Cf(sf)
v_L / v_H	1.395/1.100	1.390/1.047	2.056/1.710

As observed in the table, the light group emits about 20-30% more neutrons than the heavy group: v_L /v_H ≈ 1.2 - 1.3.

The total neutron multiplicity vtot (A)> for a given mass fragmentation is found by summing the emission numbers <v(A)> of complementary fragments. The total multiplicity is seen in the figure for ^{235}U(n_{th},f) to peak at mass symmetry (open circles). Since the total available energy Q* = TKE* + TXE has to be shared between the kinetic and the excitation energy, the peak in the total neutron emission in Fig. 44 corresponds to the peak in total excitation energy in Fig. 22 or the dip in total kinetic energy in Fig. 21, respectively.

The investigation both in experiment and theory of the energy spectra of neutrons from fission has a long history and is still going on. To good approximation it is assumed that in low energy fission the bulk of neutrons is evaporated from the fragments having reached their full speed. Fragments reach 90% of their final velocity in ≈ $5x10^{-21}$ s while neutrons are evaporated in times > 10^{-19s}. For example, to evaporate a neutron with energy E_n = 1 MeV takes 10^{-18} s.

In experiment neutrons and their spectra are measured in the Lab system. From theory one expects that the transformation of an evaporation spectrum in the Centre of Mass system of fragments yields a Watt spectrum in the LAB. Somewhat surprisingly it turns out that in the LAB a Maxwell spectrum describes well the measured spectra of neutron energy E_n:

$$\Phi(E_n) \quad E_n^{1/2} \exp(-E_n/T) \qquad (20)$$

with $\langle E_n \rangle = (3/2)\,T$ and $\sigma^2 = 2\langle E_n \rangle^2 / 3$.

As demonstrated in Figs. 45, the global spectrum for ^{252}Cf(sf) is well described by a Maxwell distribution [40). From a fit to the data the temperature parameter is found to be T = 1.42 MeV. This corresponds to an average energy $\langle E_n \rangle$ = 3/2 T = 2.13 MeV. The peak energy E_p is E_p = T/2 = 0.71 MeV. The data are shown both on a linear (a) and a logarithmic energy scale (b) for the neutrons. On the linear scale the exponential decrease of neutron yield for energies E_n in excess of E_n ≈ 2 MeV is evident. On the logarithmic scale more details of the low energy part of the spectrum come into view.

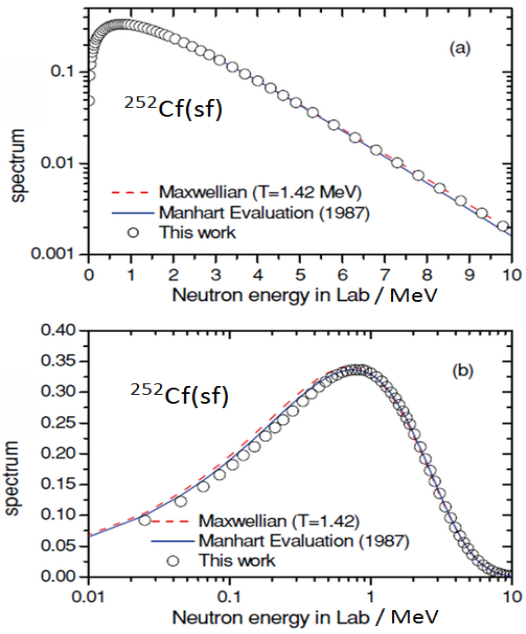

Fig. 45: Spectrum of neutrons from ^{252}Cf(sf) in the Laboratory (LAB system)

An important role in the discussion of neutron spectra plays the Manhart evaluation [41] shown in the figure. It combines the work of several authors. The spectrum often serves as a reference.

In the figures besides the Manhart spectrum and its fit to a Maxwellian also theoretical results are displayed as open circles 40]. The starting point for theory is the evaporation spectrum of neutrons as derived by Weisskopf [42]. The spectrum for one neutron emitted in the CM of the moving fragment is given by

$$(\eta) \quad (\eta/T^2) \exp(-\eta / T) \qquad (21)$$

with η the kinetic energy of neutrons in the CM system and T the temperature of the daughter nucleus. For the calculations the temperatures of the two fragments have to be known. A major difficulty in the analysis is the fact that the cascades of neutrons emitted have to be followed neutron by neutron. The resulting Watt spectrum is clumsy.

In experiment the transformation between Lab and CM system is tackled the other way round. It is conjectured that the bulk of prompt neutrons are evaporated isotropically from fragments having reached their full final speed. Evidence comes from the analysis of velocities and angular distributions of neutrons relative to the fission axis as observed in the LAB system. In the LAB the velocity distribution is markedly non-isotropic: the neutron density as a function of velocity and angle relative to the fission axis is strongly shifted in direction of fragment flight. It is attributed to the isotropic distributions of neutron velocities in the CM systems of fragments. This kinematical anisotropy in the LAB system comes about by the vector addition of neutron and fragment velocities. The transformation of neutron spectra form the LAB to the Centre-of-Mass (CM) system of fragments and vice versa is illustrated in Fig. 46.

For the transformation of neutron spectra from the Cm to the LAB system the fragment velocities have to be known. In experiment neuron emission and fragment energies have to be measured in coincidence. This allows in Fig.46 the transformation of neutron velocities and angles event by event form the LAB to the CM system of neutron emission back and forth.

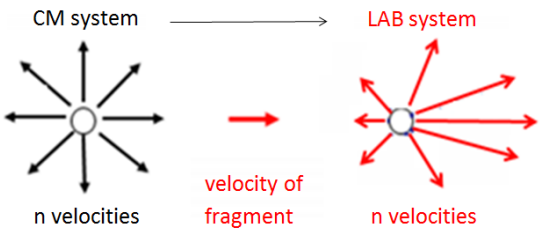

Fig. 46: The transformation from the CM to the LAB (and vice versa) of neutron velocity and angular distributions is a simple Galilei transformation

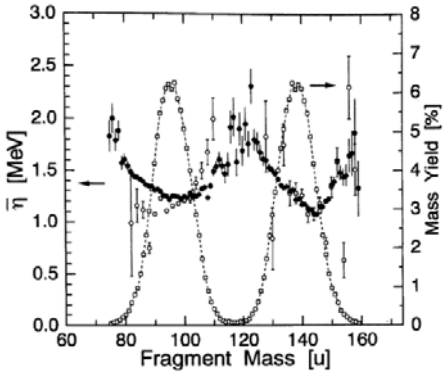

Fig. 47: Average CM neutron energy as a function of fragment mass in $^{233}U(n_{th},f)$

The neutron energy spectra in the CM system of fragments thus determined are for all fragment masses well approximated again by a Maxwellian distribution:

$$(\eta) \quad ^{1/2} \exp(-\eta / T_{eff}) \qquad (22)$$

Hereby T_{eff} is to be understood as an effective temperature over the emission cascade of neutrons. An example for the reaction $^{233}U(n_{th},f)$ is provided in Fig. 47 [36]. The average neutron energies $<\eta(A)>$ as a function of fragment mass A are on display. For comparison also the mass yields are given. On average for the light and heavy mass group the energies are $<\eta> \approx 1.3$ MeV. For symmetric and super-asymmetric fission the CM energies reach maxima with $<\eta(A)>$ close to 2 MeV. The large excitation energies in Fig. 22 for these two mass regions hence not only reflect the large total neutron numbers (see Fig. 44) but also the large neutron energies.

It is worth noting that in the Maxwell distribution of eq. (22) the effective temperature $T_{eff} = 2/3 <\eta>$ becomes $T_{eff} \approx 0.87$ MeV for the reaction $^{233}U(n_{th},f)$. For the reaction $^{252}Cf(sf)$ the temperature is evaluated to be $T \approx 1.0$ MeV [36]. These are thermodynamic temperatures of fragments while the temperature parameter T = 1.42 MeV found for the Manhart spectrum in Fig. 45 in the laboratory is a parameter but not a temperature in the usual sense.

With the knowledge of the neutron energies in the CM system in which they are evaporated it is now possible to find the total excitation energy drained by neutrons $<E_{ntot}>$:

$$<E_{ntot}> = <\nu_{tot}> (<B_n> + <\eta>) \qquad (23)$$

with $<B_n> \approx 5.5$ MeV the average neutron binding energy in the fragments. One thus obtains for $^{235}U(n_{th},f)$ the energy $<E_{ntot}> \approx 17$ MeV and for $^{252}Cf(sf)$ the energy $<E_{ntot}> \approx 26$ MeV. These figures were used in eq. (13) and Fig. 19 to find the total excitation energy TXE.

There is one simple analytical relation between neutron energies in the LAB and in the CM which should be indicated though in general the transformation laws between neutron spectra in the two systems lead to rather complex expressions. For the global average energies $<E_n>$ in the LAB and $<\eta>$ in the CM, and with E_F the fragment kinetic energy per nucleon the relation holds:

$$<E_n> = <\eta> + <E_F> \qquad (24)$$

The discussion of neutron emission in low energy fission having been given here covers only the most basic facts. Modern research is focused on issues like the existence of neutrons ejected right at scission and the anisotropy of neutron emission in the CM due to angular momentum carried by the fragments.

Probabilities for fission in reactions with MeV neutrons should be briefly addressed. Irradiating heavy nuclei in the actinides with very low energy neutrons, e.g. thermal neutrons, the absorption of a neutrons leads to the always present capture (n,γ) reaction and in case of fissile target nuclei in addition to the fission reaction (n,f). At higher incident energies in the MeV range, following neutron capture fission has to compete with neutron re-emission. This is schematically illustrated in Fig. 48 for an e-e compound nucleus. E* is the excitation energy of the nucleus. In the fission sector to the right B_f, Δ_f, and ε are the fission barrier, the pairing energy gap in the level density of the fissioning nucleus and the kinetic energy in the fission degree of freedom at the saddle, respectively. The intrinsic energy of excitation at the saddle point is $(E^* - B_f - \varepsilon)$. In the neutron sector to the right, B_n is the binding energy while $(E^* - B_n)$ is the excitation energy of the daughter nucleus having evaporated a neutron. The relative probabilities of decay are quantified by the decay widths Γ_f and Γ_n for fission and evaporation, respectively. The relative probabilities of decay are approximately given by

$$\Gamma_n/\Gamma_f \quad \exp\{-(B_n - B_f)\} \qquad (25)$$

For fissile nuclei like ^{236}U*the difference is $(B_n - B_f) > 0$ (see Fig. 48) while for fertile nuclei like ^{238}U one has $(B_n - B_f) < 0$.

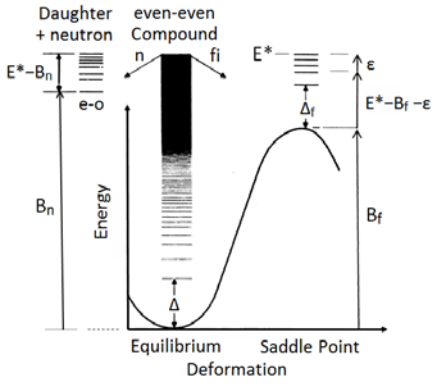

Fig. 48: Level scheme for an e-e fissile nucleus like 236U* as a function of deformation towards fission [43].

It should be recalled that besides the (n,f) and the (n,γ) reactions, where the incoming neutron is absorbed, neutrons may be scattered elastically or inelastically in (n,n) or (n,n`) reactions.

A typical example for the fission cross section (n,f) at higher excitation energy is on display in Fig. 49 for the target ^{238}U. The stepwise increase of the cross section with incident neutron energy is startling. The explanation is straightforward. For the non-fissile nucleus ^{238}U the fission barrier is $B_f \approx 6.1$ MeV and thus larger than the neutron binding $B_n \approx 4.8$ MeV gained by neutron capture. For the fission cross to become sizable the missing 1.3 MeV have to be supplied by the kinetic energy of the incoming neutron. Further increasing the neutron energy the cross section stays constant for about 5 MeV until a second step at ≈ 6.5 MeV indicates that the threshold for a new process has been reached. In the new process a neutron may be emitted from the compound ^{239}U but still enough energy being left to overcome the fission barrier of the daughter ^{238}U. There are thus two processes contributing to fission: "first chance fission " (n,f) and "second chance fisssion" (n,n´f).

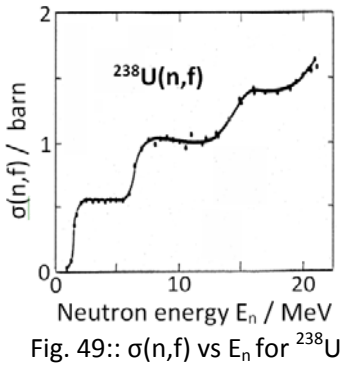

Fig. 49:: σ(n,f) vs E_n for ^{238}U

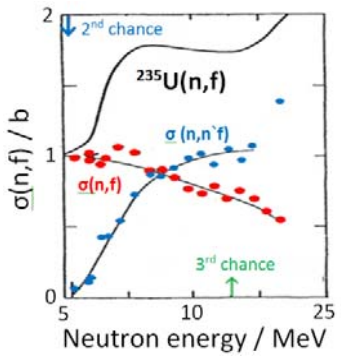

Fig. 50: σ(n,f) vs E_n for ^{235}U

Similar to Fig. 49, in Fig. 50 [44] the multi-chance fission cross section for the reaction ^{235}U(n,f) with the fissile isotope ^{235}U is presented. At higher incoming neutron energies E_n a stepwise increase of the cross section like in the reaction 238U(n,f) is found. The figure shows further in the overlap of first and second chance fission the individual contributions. As soon as sufficient incoming energy E_n is made available, second chance fission σ(n,n`f) starts to rise while first chance fission σ(n,f) is fading away.

The (n,f) fission cross section has been studied for several actinide isotopes up to neutron energies of several 100 MeV.

Most neutrons are evaporated in times smaller than a few 10^{-14} s. These are called the prompt neutrons studied in the foregoing. A second fraction of neutrons is showing up at much later times starting at about 1 ms after fission. These late neutrons are therefore called "delayed neutrons".

After prompt neutron emission the primary fragments have become fission products. As a rule these latter nuclei are still too n-rich and hence unstable. To reach the stability line of the nuclide chart they undergo β^--decay. The β-decay is induced by the weak interaction and the corresponding reaction times are long. For fission products showing up in fission the β^--decay times range from 1 ms to times longer than the age of the universe. For many of the fission products β^-decay leads in the daughter nuclei to excitation energies in excess of the neutron binding energy. In these cases-besides delayed gammas- also delayed neutrons may be emitted.

In emission of delayed neutrons the nuclei involved are the n-precursor fragment ${}^{A}_{Z}\mathbf{X}_{N}$, following β-decay the neutron emitter ${}^{A}_{Z+1}\mathbf{Y}_{N-1_1}$ and following n-emission the final product ${}^{A-1}_{Z+1}\mathbf{Y}_{N-2}$+ **n.** The level schemes illustrate cases favorable for the emission of delayed neutrons.

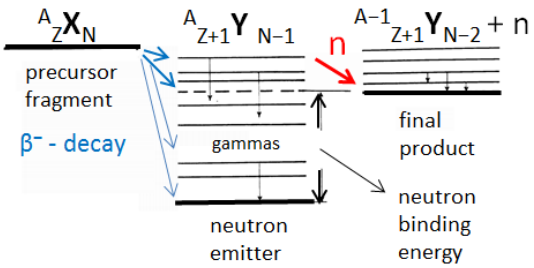

Fig. 51: Level schemes in delayed neutron emission

The number N_β of β-decays per fission in (n_{th},f)-reactions of actinides is N_β= 6.0 0.5. Among the fission products about 300 nuclei are precursors to emission of neutrons. Most delayed neutrons appear within 1 min after fission. They are of crucial importance for the safe operation of power reactors. To simplify the analysis they are lumped together into 6 groups according to their half-lives $T_{½}$. Delayed neutron data are given in the table. The characteristic parameters are the half-life $T_{½}$, average neutron energies $<E_n>$ and probabilities P_k in % for the six groups labeled k. They are shown in the table [38].

k	$T_{1/2}$ /s	E_n/MeV	P_k /%
1	53.0	0.41	3.5
2	21.6	0.47	18.1
3	5.3	0.44	17.3
4	2.3	0.56	38.7
5	0.83	0.52	15.6
6	0.25	0.54	6.6

Averaged over all groups the half-life for delayed neutrons from thermal fission of ^{235}U is $T_{½}$ = 9(1) s. This time span is sufficient to stop a reactor by inserting control rods into the reactor core.

The energy spectra of delayed neutrons are parameterized as Maxwellians with a temperature of T = 0.34 MeV and an average energy E_n of $<E_n>$ = 0.51 MeV.

For the safe operation of power reactors not only the half-lives of delayed neutrons are a crucial parameter. The percentage of delayed neutrons is likewise important since it governs the flexibility of reactor operation. For thermal neutron fission of ^{235}U and ^{239}Pu the ratio $\beta = \nu_{del}/\nu_{tot}$ of delayed to total neutron numbers with $\nu_{tot} = \nu_{prompt} + \nu_{del}$ is β = 0.65% and β = 0.24%, respectively.

5b. Gammas

The bulk of gammas from fission are emitted following neutron evaporation as shown in Fig. 40. The number of gammas called the γ-ray multiplicity and the total energy set free by gammas $E_{\gamma tot}$ is of prime

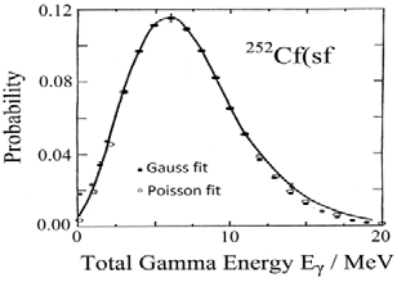

Fig. 52 to the left: Total prompt γ-energy for ^{252}Cf(sf) [44]

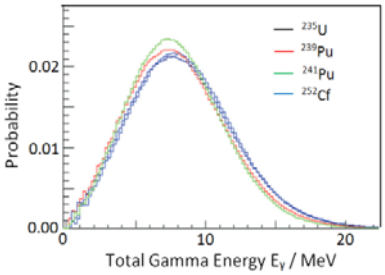

Fig. 53 to the right: Total prompt γ-energy in (n_{th},f) of ^{235}U, ^{239}Pu and ^{241}Pu [45]

interest. For ^{252}Cf(sf) in Fig. 52 the γ-energy was accumulated during 30 μs after scission in a NaJ detector. On average the energy is quoted to be $\langle E_{\gamma tot}\rangle$ = 7.1 MeV. The contribution by gammas later than 30 μs is negligible.

In a comparative study of low energy n-induced fission of ^{235}U, ^{239}Pu and ^{241}Pu, and spontaneous fission of ^{252}Cf the total γ-ray energy E_γ was measured with the spectrometer DANCE from LANSCE in a time window of 40 ns after fission. As γ-detectors served 160 BaF scintillators. As borne out in Fig. 53 the figure, the distributions of E_γ for the four reactions analyzed are very similar. A remarkable result is obtained for the average total γ-energy $\langle E_{\gamma tot}\rangle$ which exceeds all former measurements by 20%. For example, for ^{252}Cf(sf) the average total gamma energy is reported to be $\langle E_{\gamma tot}\rangle$ = 8.52 MeV. Taking the short time window of gamma observation into account this figure is rather a lower limit to the γ-energy release. Since prompt gammas contribute to the heating of reactor cores a precise knowledge of the energy release $\langle E_{\gamma tot}\rangle$ is of great practical importance. More precise and reliable data are still required.

Discussing the total available excitation energy TXE in fission the relation for TXE = E_{ntot} + $E_{\gamma tot}$, viz. TXE = $\nu_{tot}\cdot(B_n + \eta]$ + $E_{\gamma tot}$ was introduced in eq. (13). The contribution by neutrons was already handled in connection with eq. (23). The contribution by gammas should finally be taken into account. For the two reactions ^{235}U(n_{th}.f) and ^{252}Cf(sf) this is done in the table:

Reaction	ν_{tot}	B_n	η	$E_{\gamma tot}$	E_{ntot} + $E_{\gamma tot}$
^{235}U(n_{th},f)	2.43	5.5	1.4	8(1)	24.8(20)
^{252}Cf(sf)	3.76	5.5	1.4	8(1)	33.9(20)

Throughout average values are given with energies in MeV. Mainly due to the γ-sector the uncertainties entail large error bars. Nevertheless it can be noted that the variations in neutron multiplicity are responsible for the different excitation energies TXE.

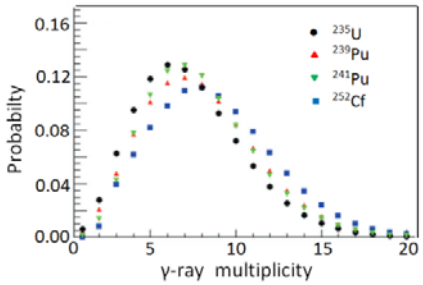

Fig. 54: Gamma multiplicities

Gamma multiplicities M_γ for thermal neutron induced and spontaneous fission are very similar. This is brought to evidence in the comparative study already addressed in connection with the total γ-energy output E_γ [45]. In the four reactions under study up to 20 γ-quanta per fission are observed. The largest differences between average multiplicities are between ^{235}U(n,f) with $\langle M_\gamma\rangle$ = 7.35 and ^{252}Cf with $\langle M_\gamma\rangle$ = 8.7

A rough estimate for the average energy $\langle\varepsilon\rangle$ of single γ-quanta is obtained from $\langle\varepsilon\rangle = \langle E_\gamma\rangle/\langle M_\gamma\rangle$. The energy is $\langle\varepsilon\rangle$=1.0(1) MeV.

Of prime interest for comparison with theory are the energies ε_γ of individual photons and their multiplicity M_γ. In recent comprehensive studies the gamma emission from ^{252}Cf(sf) was studied and compared to data taken 40 years earlier. Gamma spectra on display in Fig. 55 were taken by different types of scintillators: NaJ(Tl) [46], BaF_2 [45] and $LaBr_3$:Ce [47]. The time window in experiment was <10 ns.

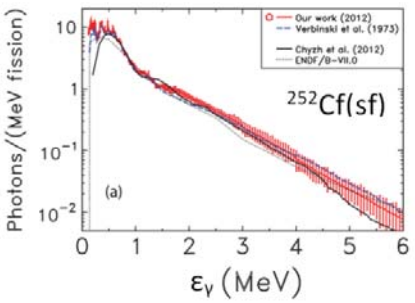

Fig. 55 to the left: Photon spectrum of ^{252}Cf(sf) as measured in experiment

Fig. 56 to the right: Photon spectrum of ^{252}Cf(sf) as calculated by theory

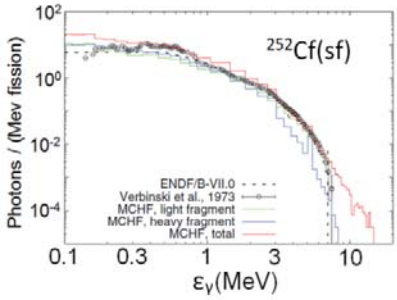

The gamma-spectrum is well described by theory as brought to evidence in the companion Fig. 56 for the same reaction ^{252}Cf(sf). Open circles are plotted as experimental reference [46]. Theoretical results from a Monte Carlo Hartree-Fock model are displayed as histograms [48].

The gamma spectrum observed in the standard reaction ^{235}U(n_{th},f) is not much different from the one for (sf) of ^{252}Cf. As seen in Fig. 57 the emission probability decreases smoothly by 4 orders of magnitude for gamma energies ε_γ from 1 MeV to 6 Mev. Only at low photon energies < 1 MeV a fine structure shows up.

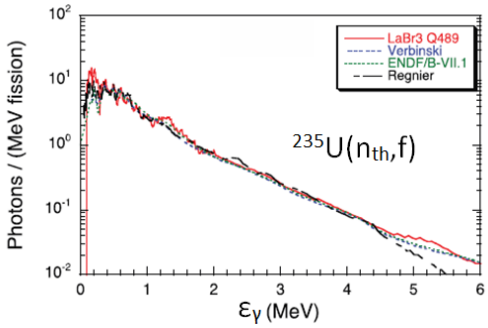

Fig. 57: Gamma spectrum for ^{235}U(n_{th},f) [45]

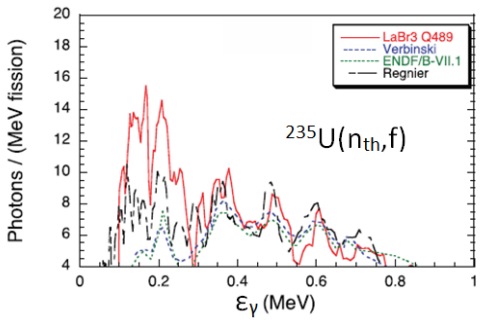

Fig. 58: Zoom of Fig. 57 for E_γ < 1 MeV

This structure becomes convincing in a zoom for gamma energies below 1 MeV in Fig. 58. The structure was already observed in 1957 [45], established in 1973 [41] and corroborated with high resolution 40 years later [46]. The structure is attributed to collective rotational levels of (e,e) fission products.

Deeper insight into the details of gamma emission is gained by investigating gamma multiplicity and photon energy for fragments with known mass. This was studied for several standard (n_{th},f) and (sf) reactions. A typical example is on display for the reaction ^{239}Pu(n_{th},f) in Fig. 59 [49]. Remarkably for a time window of less than 5 ns the multiplicity M_γ in the top panel of the figure has the same sawtooth behaviour as the neutron multiplicity ν_n. They have in fact as a common root the deformation of fragments at scission. Take e.g. the light fragment mass A_{LF} = 110 in ^{240}Pu*: for neutrons it is the large energy stored in the large deformation which is counting while for gammas the large deformation primarily leads to large angular momenta of fragments. The large momenta have subsequently to be exhausted by more than average numbers of photons.

The total average gamma energy <E_γ(A)> per fragment in the bottom panel of Fig. 59 also follows in shape a sawtooth as a function of mass, but the structure is much less pronounced. The reason is found in the particular behaviour of the quantum energy ε_γ(A) as a function of mass A.

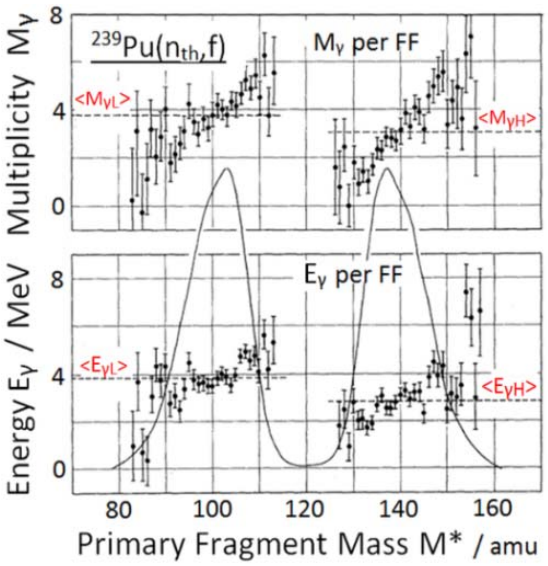

Fig. 59: On top and bottom multiplicity $M_\gamma(A)$ and total gamma energy $E_\gamma(A)$ for $^{239}Pu(n_{th},f)$

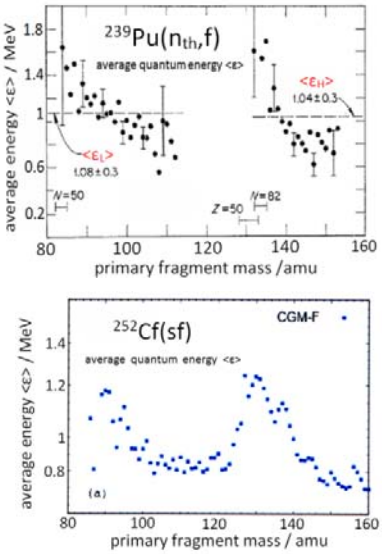

Fig. 60: Experimental photon energy $\varepsilon_\gamma(A)$ for $^{239}Pu(n_{th},f)$ and theory for $^{252}Cf(sf)$

In contrast to γ-multiplicity $M_\gamma(A)$ the plot of the quantum energy $<\varepsilon(A)>$ *vs.* fragment mass looks like an anti-saw-tooth. This is visualized in Fig. 60, on top from experiment for $^{239}Pu(n_{th},f)$[49] and on bottom for ^{252}Cf from theory [47]. While for magic fragments near $A_{HF} = 132$ and near $A_{LF} = 80$ the multiplicities $M_\gamma(A)$ are small, the photon energies $\varepsilon_\gamma(A)$ are large. Obviously the wider level spacing for magic fragments entails low γ-multiplicity but large quantum energies $<\varepsilon(A)>$. The total gamma energy is $<E_\gamma(A)> = <M_\gamma(A)> \cdot <\varepsilon_\gamma(A)>$ and therefore a rather flat as a function of fragment mass A.

The actinides ^{233}U and ^{235}U in thermal neutron fission and ^{252}Cf in spontaneous fission exhibit similar features for the photon energy $\varepsilon_\gamma(A)$ of fragments. As shown in the bottom panel of Fig. 60 for $^{252}Cf(sf)$the structure of $\varepsilon_\gamma(A)$ is well understood by theory [50].

A special topic in γ-emission is the **anisotropy of gamma emission**. Unlike isotropic emission for the bulk of neutrons, γ-emission is non-isotropic relative to the fission axis. This was found for all low energy fission reactions studied. An example is on display in Fig. 61 for ^{252}Cf (sf) [51]. The anisotropy A is defined as

$$A = [W(0°) - W(90°)]/W(90°) \qquad (25)$$

with emission probabilities $W(\theta_{\gamma f})$ at the angle $\theta_{\gamma f}$ between gamma and fission axis.

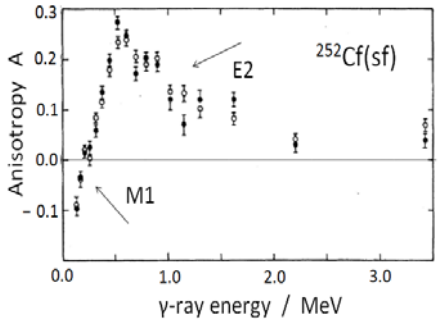

Fig. 61: Gamma anisotropy for $^{252}Cf(sf)$ [51].

The anisotropy measured varies strongly with γ-energy. For low-energy gammas with $E_\gamma < 200$ keV the anisotropy A is $A < 0$ with more gammas emitted at $\theta = 90°$ perpendicular to the fission axis than along the fission axis at $\theta = 0°$. The anisotropy changes sign for the majority of gammas with energies $E_\gamma > 200$ keV. For positive $A > 0$ gammas are preferentially emitted along the fission axis.

A succinct interpretation of the anisotropy was given by V. Strutinski in 1960 [52]. It is pointed out that the sizable angular momenta carried by the fragments are oriented in a plane perpendicular to the fission axis. The probability for emission of gammas is basically a function of the angle $\theta_{\gamma I}$ between the

gamma and fragment spin I. The spin I of fragments is not accessible event by event in experiment. What is observed in γ-emission is the average over all orientations of spin around the fission axis. After averaging the angular distribution $W(\theta_{\gamma I})$ becomes a function $W(\theta_{\gamma f})$ of the angle $\theta_{\gamma f}$ between the gamma and the fission axis in the CM system of the fragment. The distribution depends on the multipole moment L of the radiation field. To each moment L belongs a characteristic angular emission pattern. According to Strutinski the angular distribution reads

$$W_{L=1}(\theta_{\gamma f}) \approx 1 + \tfrac{1}{8}(\hbar^2 I/\quad T)^2 \sin^2\theta_{\gamma f} \text{ for L = 1 (dipole)} \tag{26a}$$

$$W_{L=2}(\theta_{\gamma f}) \approx 1 - \tfrac{3}{8}(\hbar^2 I/\quad T)^2 \sin^2\theta_{\gamma f} \text{ for L = 2 (quadrupole).} \tag{26b}$$

Note that the anisotropy A is negative for dipole and positive for quadrupole radiation. This could explicitly be verified by analyzing the anisotropy for single transitions between known levels in the ^{252}Cf(sf) reaction. This is shown in Fig. 62 [53]. To the left the M1 dipole gammas to the ground state of

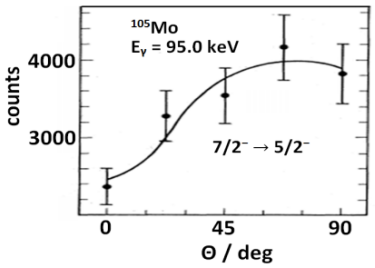

Fig. 62a to the left: Angular distribution of dipole gammas from ^{105}Mo in ^{252}Cf(sf) [53]

Fig.62b to the right: Angular distribution of quadrupole gammas from ^{144}Ba in ^{252}Cf(sf) [53]

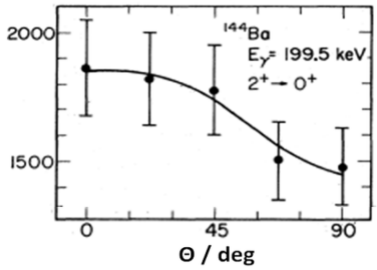

^{105}Mo are preferentially emitted perpendicular to the fission axis, while the E2 quadrupole gammas to the groundstate of ^{144}Ba favor emission along the fission axis. It has to be pointed out that the above angular distributions from theory pertain to the emission in the CM system of fragments while the experimental results are obtained in the LAB system. Yet the transformation from the CM to the LAB system will not change the characteristics of the gamma angular distributions.

Finally gammas emitted in times after about 50 ns after fission should be inspected. Gammas emitted later than about 50 ns may be called **late gammas**. They should not be confounded with β-delayed gammas emitted following β-decay by daughter nuclei left in an excited state. Late gammas presently to be discussed stem from isomeric states of fragments having been excited in the course of fission.

Searching for late gammas, in a study of spontaneous fission of ^{252}Cf the time window of γ-detection was extended from 3 ns to 2000 ns [54]. In Fig. 63 γ-spectra taken in the time range 10 ns to 2000 ns is on view. Remarkably, long-living isomers, albeit with small yields, show up for two different ranges of γ-energy: for low energies below 500 keV and for very high energies near 1250 keV. It is further found that these γ`s are preferentially emitted from fragments near mass 132. This mass number suggests the influence of magic shells like in ^{132}Sn. Microsecond isomers in the magic regions ^{78}Ni and ^{132}Sn have been extensively studied in recent years [55].

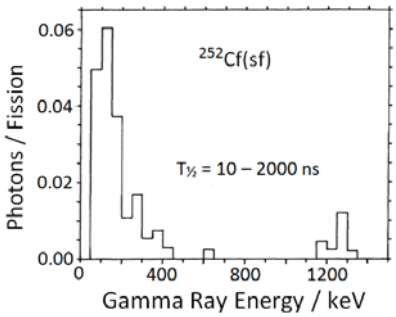

From the γ-anisotropy measurements discussed in the foregoing it is concluded that these high energy gammas have the multipolarity E2. They may possibly be interpreted as collective vibrations of stiff magic nuclei. However, they are by orders of magnitude slower than anticipated. Most probably their origins are either spin or shape isomers at the head of γ-cascades. The topic "late gammas" has so far not been adequately explored.

Fig. 63: Late gammas from ^{252}Cf(sf)

There is finally a further source of gammas, the so-called **delayed gammas**. Following prompt neutron and prompt gamma emission all the TXE is exhausted and the primary products have reached their ground states. However, as already discussed in connection with the topic "delayed neutrons", these states are not β^- stable. The reason is simple: for heavy nuclei like fissioning actinides the N/Z ratio for the compound is larger than for the medium-weight fission fragments. Yet the available TXE is not sufficient to evaporate enough neutrons. Take symmetric fission of $^{235}Un_{th}$,f) as an example. The two primary fragments are $^{118}Pd_{72}$. The energy at disposal is about TXE = 40 MeV. Per fragment this allows the evaporation of 2 neutrons. The two final products $^{116}Pd_{70}$ in Fig. 64 arrive at the ground state after 10^{-14} s for neutron evaporation and <1 ms for prompt gamma emission. These isotopes are unstable with a half-life of 11.8 s for a first β^-decay to $^{116}Ag_{69}$, decaying further with half-lives up to 2.7 m to the stable Cd isotope $^{116}Cd_{68}$. Each β^--decay is accompanied as a rule by γ-rays, the "delayed gammas".

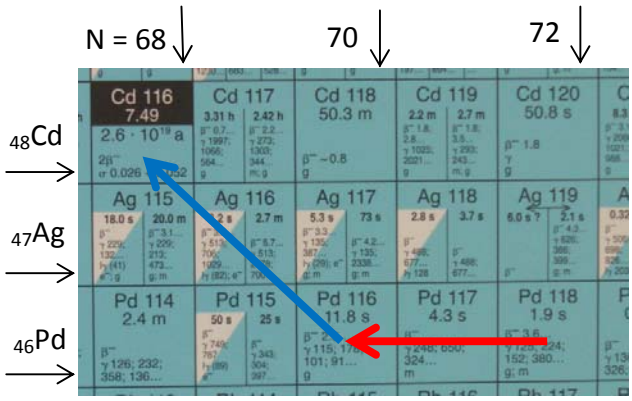

Fig. 64: Zoom of the chart of nuclides showing neutron emission (red arrow) and β^-decay (blue arrow) on the path from $^{118}Pd_{72}$ to $^{116}Cd_{70}$.

On average there are 6 β^-decays per fission. While there are only very few delayed neutrons (≈1 delayed neutron per 60 fission events in $^{235}U(n_{th},f)$), there is a large amount of gammas. Together with the β-particles they are responsible for the radioactivity of burnt fuel elements from nuclear power stations.

6. Summary

The essence of nuclear fission is deformation of a nucleus up to a saddle point in deformation space, the so-called fission barrier. Once the saddle has been passed, deformation is further increasing and leading eventually to scission into two fragments. The basic theory is based on the Liquid Drop Model with corrections for nuclear structure viz. shell and pairing effects. In the actinides the height of the fission barrier is ≈6 MeV. Neutron induced fission was almost exclusively studied with actinides as targets. For many isotopes the neutron binding energy exceeds the barrier and fission becomes observable with thermal neutrons.

Outstanding features of the fission fragments are their mass, charge and energy distributions. At low excitation energies the mass distributions are asymmetric in the actinides from Ac to Fm. The asymmetry is due to the stabilizing effect of magic nuclei like ^{132}Sn for standard asymmetric and ^{78}Ni for superasymmetric fission. For heavy Fm isotopes up to Lr and beyond mass distributions are symmetric. In this mass region symmetric bimodal fission is observed. Distinct modes in the mass distributions Y(A;E) are highlighted by constraining fragment energy E. They are linked to distinct paths of the nucleus in the potential energy surface between saddle and scission. Charge distributions of fragments follow rather closely the mass distributions. A particularity, however, is a pronounced even-odd staggering in the charge yields. The e-o effect is traced partly to superfluidity and partly to fragment shells.

The total energy set free in fission is shared between the total kinetic and the total excitation energy of fragments. The excitation energy is exhausted by the emission of neutrons and gammas. A salient feature in neutron and gamma emission is the saw-tooth like shape of the multiplicities as a function of mass. It is due to different deformabilities and thus energy storage capacities and/or angular momenta

of fragment nuclei. In the γ-decay a characteristic feature is the anisotropy of γ-emission relative to the fission axis. It is traced to the angular momentum the fragments get imparted at scission. For neutrons the influence of angular momentum is less pronounced. In the CM systems of fragments the bulk of neutrons are emitted isotropically with only a small fraction of neutrons being evaporated non-isotropically.

Following neutron and gamma emission the fission products are in their ground state. However they are unstable against β^--decay. Per fission there are about 6 β^-decays with emission of betas and anti-neutrinos. The radioactivity of burnt fuel elements of power reactors is due to these betas and the accompanying gammas. In β-decay occasionally also delayed neutrons are ejected. These neutrons play a crucial role for the safe operation of reactors.

References

[1] S. Björnholm and J.E. Lynn: Rev. Mod. Phys. 52, 725 (1980)
[2] J.P. Unik, J.E. Gindler, J.E. Glendenin et al.: Proc. "Phys. and Chem. of Fission" IAEA Vienna , Vol II, 20 (1974)
[3] E. Konecny, H.J. Specht and J. Weber: Proc. "Phys. and Chem. of Fission" IAEA Vienna, Vol II, 3 (1974)
[4] S. Nagy, K.F. Flynn, J.E. Gindler et al.: Phys. Rev. C 17, 163 (1978)
[5] V. Pashkevich: private communication
[6] P. Möller, A.J. Sierk, T. Ichikawa et al.: Phys. Rev. C 79, 064304 (2009)
[7] H. Goutte, J.F. Berger, P. Casoli et al.: Phys. Rev. C 71, 024316 (2005)
[8] E. Pfeiffer : Z. Physik 240, 403 (1970)
[9] F.J. Hambsch, S. Oberstedt, A. Tudora et al.: Nucl. Phys. 726, 248 (2003)
]10] U. Brosa, S Grossmann and A. Müller: Phys. Reports 197, 167 (1990)
[11] H.H. Knitter, F.J. Hambsch, C. Budtz-Jorgensen et al.: Z. Naturf. 42a 786 (1987)
[12] L. Dematté, C. Wagemans, R. Barthélémy et al.: Nucl. Phys. A 617, 331 (1997)
[13] D. Rochman, I. Tsekhanovich, F. Gönnenwein et al.: Nucl. Phys. A 735, 3 (2004)
[14] I. Tsekhanovich, H.-O. Denscjhlag, M. Davi et al.: Nucl. Phys. A 688, 633 (2001)
[15] K. Hulet: Phys. At. Nucl. 57, 1099 (1994)
[16] P. Geltenbort: PHD thesis, Univ. Tübingen, 1985 unpublished
[17] J.C.D. Milton and J.S. Fraser: Phys. Rev. 111, 877 (1958)
[18] F. Gönnenwein: in "The Nuclear Fission Process", C. Wagemans ed. CRC Press 1991
[19] A. Ruben and H. Märten: Proc. "Dynamical Aspects of Nuclear Fission", Dubna 1992
[20] H.W. Schmitt, J.H. Neiler and F.J. Walter: Phys. Rev. 111, 1146 (1966)
[21] W. Mollenkopf, J. Kaufmann, F. Gönnenwein et al.: J. Phys. G 18, L203 (1992)
[22] J.P. Bocquet and R. Brissot: Nucl. Phys. 502, 213c (1989)
[23] ILL collaboration in H. Börner and F. Gönnenwein: "The Neutron", World Scientific, Singapure (1992)
[24] P. Schillebeeckz, C. Wagemans, P. Geltenbort et al.: Nucl. Phys. A 580, 15 (1994)
[25] F. Gönnenwein in "The Neutron" by H. Börner and F. Gönnenwein, World Scientific, Singapure (1992)
[26] G.D. Adeev and I.I. Gonchar: Z. Physik A422, 479 (1985)
[27] M. Asghar and R. Hasse: J. Physique C 6, 455 (1984)
[28] J.L. Sida, P. Armbruster, M. Bernas et al.: Nucl. Phys. 502, 233c (1989)
[29] D. Hilscher and H. Rossner: Ann. Phys. (Paris) 17,471 (1992)
[30] J. Terrell: Phys. Rev. 108, 784 (1957)
[31] A.S. Vorobyev, V.N. Dushin, F.-H. Hambsch et al.: "Interactions of Neutrons with Nuclei", Dubna 2001, 276
[32] V.P. Zakharova, D.K. Ryazanov et al. Nucl. Phys. 30, 19 (1979)
[33] C. Signarbieux, J. Poitou, M. Ribrag et al.: Phys. Lett. 39B 503 (1972)
[34] R.I. Walsh and J.W. Boldeman: Nucl. Phys. A 276, 189 (1977)

[35] C. Budtz-Jörgensen and H.H. Knitter: Nucl. Phys. A 490, 307 (1988)[36]
[36] K. Nishio, Y. Nakagome, H. Yamamoto et al.: Nucl. Phys. A 632, 540 (1998)
[37] E.E. Maslin, A.L. Rodgers and W.G.F. Core: Phys. Rev. 164 1520 (1967)
[38] R. Müller, A.A. Naqvi, F. Käppeler and F. Dickmann: Phys. Rev C 29, 885 (1984)
[39] A.S. Vorobyev, O.A. Shcherbakov, Yu.S. Pleva et al.: "Interactions of Neutrons with Nuclei", Dubna 2009, 60
[40] O. Litaize and O. Serot: Phys. Rev. C 82. 054616 (2010)
[41] W. Manhart in IAEA Report IAEA-TECDOC-410, 158 (1987)
[42] V.F. Weisskopf: Phys. Rev. 52, 295 (1937)
[43] R. Vandenboscch and J.R. Huizenga: "Nuclear Fission" Academic Press 1973
[44] J. Fréhaut: "Nuclear Data for Science and Technology", Mito Japan 1988, IAEA 1989, 99
[45] A. Chyzh, C.Y. Wu, E. Kwan et al.: Phys. Rev. C 90,014602 (2014)
[46] V.V. Verbinski, H. Weber and R.E. Sund: Phys. Rev. C 7, 1173 (1973)
[47] A. Oberstedt, T. Belgya, R. Billnert et al.: Phys. Rev. C 87, 051602 (2013)
[48] R. Becker, P. Talou, T. Kawano et al.: Phys. Rev, C 87, 014617 (2013)
[49] F. Pleasonton: Nucl. Phys. A 213, 413 (1973)
[50] P. Talou, T. Kanon and I. Stet: Phys. Proc. 47, 39 (2013)
[51] K. Skarsvag: Phys. Rev. C 22, 638 (1980)
[52] V. M. Strutinski: JETP Lett. 10, 163 (1960)
[53] J.B. Wilhelmy, E. Cheifetz, R.C. Jared et al.: Phys. Rev. C 5, 2041 (1972)
[54] W. John, F.W. Guy and J.J. Wesolowski: Phys. Rev. C 2, 1451 (1970)
[55] J.A. Pinston and J. Genevey: J. Phys. G. 30, R57 (2004)